Computer Assisted Mechanics and Engineering Sciences, 4: 95–126, 1997.

About the global picture of stability of equilibrium states of geometrically nonlinear deformable systems

David Shilkrut
Department of Mechanical Engineering, Ben-Gurion University of the Negev, Beer-Sheva, Israel

(Received May 27, 1996)

Despite the long history of the theory of stability of deformable system, many basic notions, statements and theorems are applied, unfortunately, not rarely incorrectly. This situation is a result of the fineness, complexity, and diversity of the phenomena connected with diverse aspects of the loss of stability of equilibrium states of nonlinear deformable systems.

The first part of the article is devoted to the attempt of elucidation of the use of a number of basic statements as the exchange of stabilities at singular points, or the effect of disappearance of bifurcation phenomena as result of geometrical imperfection of the system, and others.

The second part of the present work deals with the method of investigation of the global picture of stability of nonlinear deformable systems subjected to multiparametrical loading. This method worked of by the author is based on the so-called "deformation map" which contains the whole information of the behaviour of the system subjected to three-parametrical loading. As a basic example taken the stability of geometrically nonlinear spherical shells subjected to transient pressure, contour external forces and temperature field. A number of new effects was revealed. The map can be applied for any nonlinear system (even non elastic) which is described by means of differential equations.

1. Local and global instability

The problem is investigated via the basic example of geometrically nonlinear axisymmetrically loaded plates and shells of revolution. Such an approach does not limit, in principle, the generality of the investigations because the above-mentioned basic model possesses the main features of geometrically nonlinear plates and shells and geometrically nonlinear deformable systems in general. The theory of stability of equilibrium states of deformable nonlinear systems deals with the change of quality (transfer from stable state to unstable one and vice versa) of the states if the parameters of external loading reach some critical values (specific for the considered system and type of loading). It is very known, since the fundamental works of Euler [1, 2, 3] published 250 years ago.

In this paper we do not consider diverse exact definitions of stability of equilibrium states (see, for example, [4, 5, and others]). We shall use the following pure engineering approach to stability. The state of mechanical systems is recognized to be unstable if small (more precisely, infinitely small) perturbations remove the system away from this equilibrium state, and it never returns to the small neighbourhood of the considered equilibrium state. In the opposite case the state is stable "in the small". But there exist states which being stable "in the small" become unstable "in the large", when nonsmall (finite) perturbations take these states away without returning them to the small neighbourhood of the initial position. It is absolutely clear that the instability in the small automatically means instability in the large and stability in the large ensures the same in the small too. But, despite the fact that instability in the small is also instability in the large, the phenomena of loss of stability in the small and in the large essentially differ physically.

In the first case the transition from the unstable equilibrium state to a new stable state takes place smoothly via bifurcation, as is qualitatively shown in Fig. 1, where: λ — loading parameter, ξ — displacement of some (nonfixed) point. Curve $\lambda(\xi)$ is a projection of the real multidimensional (or even infinitely dimensional) deformation curve on plane (ξ, λ). It is clear that the number of

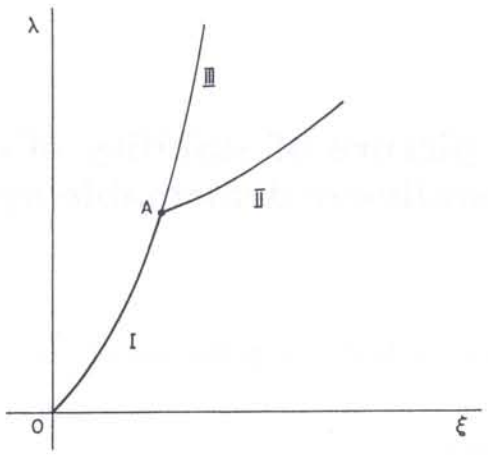

Fig. 1

such curves coincides with the number of dimensions (degrees of freedom) of the system and each curve is determined by selected displacement ξ, which is taken as the argument of function $\lambda(\xi)$. In Fig. 1 black lines depict the stable branches I and II which are joined by bifurcation point A. Light line III is the postbifurcation unstable branch. The transition to postbifurcation stable II which happens at point A is of a quasistatic type.

The opposite case (loss of stability in the large) is described qualitatively in Fig. 2. Loss of stability happens dynamically by snap-through via limit point (points A or B in Fig. 2a) or through a bifurcation point when the postbifurcation branch II is unstable (see Fig. 2b), being down directed. In the latter case the bifurcation point plays the role of a trigger of the jumping process.

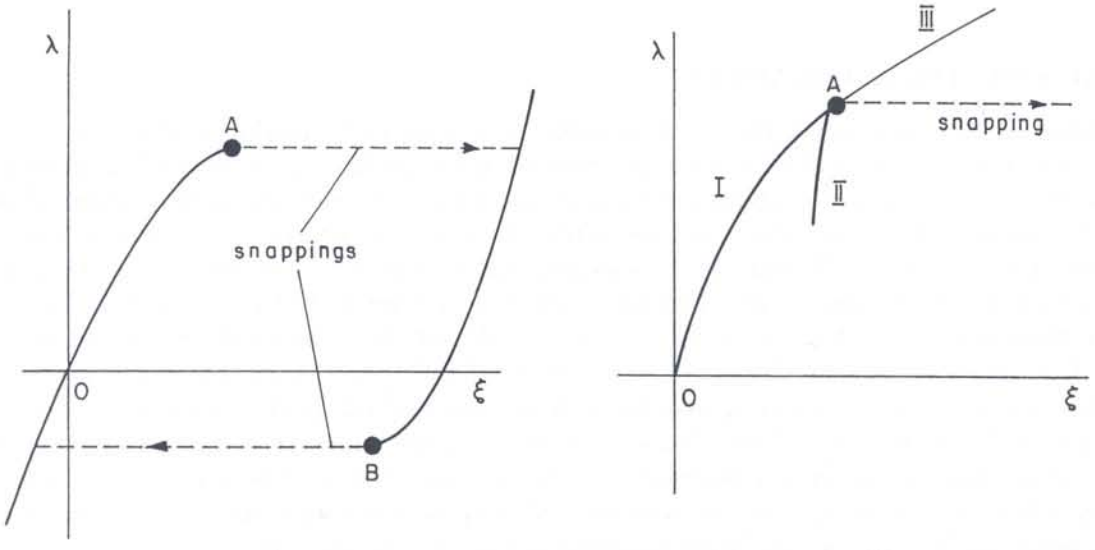

Fig. 2

Of course there exist more complicated cases than that shown in the above-given figures, but they are combinations of the two basic types of stability loss described. It is worth mentioning the following two things here. First of all let us consider the expression "linear stability" which is often met in different publications. The problem of stability loss is in principle a nonlinear problem, since in the postcritical stage there exists more than one equilibrium state, i.e. the solution of the problem is nonunique. Linear stability is used when the precritical (prebuckling) states are obtained by the

corresponding linear theory (for example linear theory of elasticity or of shells). Another use of the above mentioned unsatisfactory terminology is the case when one obtains the bifurcation points by means of linearized equations of stability (equations of neutral equilibrium). Both above-mentioned linear approaches can obtain (with corresponding accuracy the values of bifurcation loading, and some information (in the simplest case — e.g. buckling of beams and rectangular or circular plates) about the magnitudes of (buckling) loading but nothing about postcritical behavior. If limit points are considered, then the "linear" stability, in general, cannot be used.

The second point which we have to mention corresponds to the so-called structural stability. Some years ago the theory of structural stability began to be intensively developed, in which the quality (robustness) of the system as a whole is investigated when some internal parameters of the system itself change [6, 7, 8, 9]. The latter problem is in a sense more general than the above-discussed stability of states and it is not the subject of the present paper. We shall only deal with the stability of equilibrium states due to the change of external control parameters, i.e. loading parameters. The problem of structure stability is a part of the so-called "sensitivity" of the system, that is, the response of the system itself when some of its external basic parameters are changes. The global picture of the stability of equilibrium states means establishing the quality (stability) of the equilibrium states of the investigated systems in all the given ranges of variations of the loading parameters.

Practically all the investigations of the stability of equilibrium states of nonlinear deformable systems published until now are of a local type. The theory of Poincaré [10, 11] and bifurcations in general [12, 13, 14], Lyapunov–Schmidt method of reduction [14], the asymptotic approach by Koiter [15, 16] and so on, are investigations of the behavior of equilibrium states in local areas around singular points of the corresponding systems of equations of continuum nonlinear systems or systems with finite numbers of degrees of freedom. Thus the global stability in the above-mentioned sense has not been *de facto* investigated. This problem is very important, as pointed out particular in [9, 17 and others], especially when loading is multiparametrical.

In case of a single parameter loading the global behavior of the nonlinear system is described by the deformation curve (path) which for the general (continual) system is a curve spanned in an infinite dimensional space or in a finite $(n+1)$ dimensional space, where: n — number of degrees of freedom. Usually this path is realised visually by the above mentioned plane curve $\lambda(\xi)$ spanned in axes λ and ξ, cf. such curves in Figs. 3–10.

Figures 3–9 describe axisymmetrical deformation of shallow geometrically nonlinear spherical caps, while in Fig. 10 case of a cylindrical panel with the data presented in the figure is considered. In all these figures on the horizontal axes ξ are marked the dimensionless vertical displacements of the central points of spherical caps or panel.

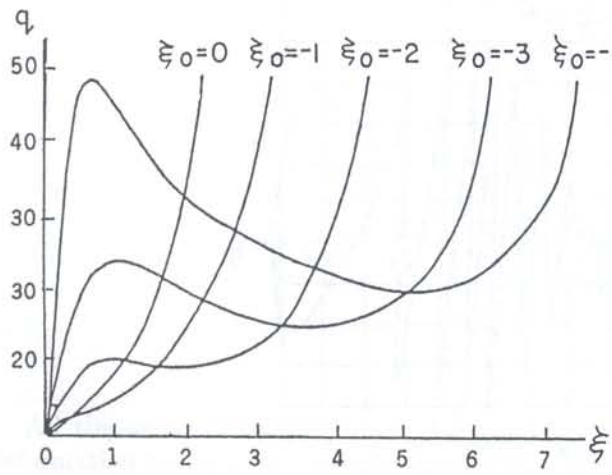

Fig. 3

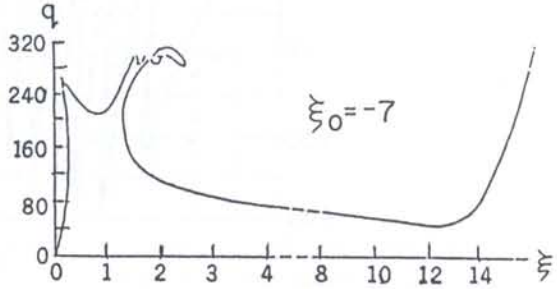

Fig. 4

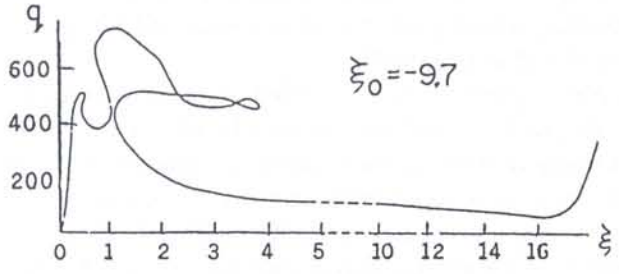

Fig. 5

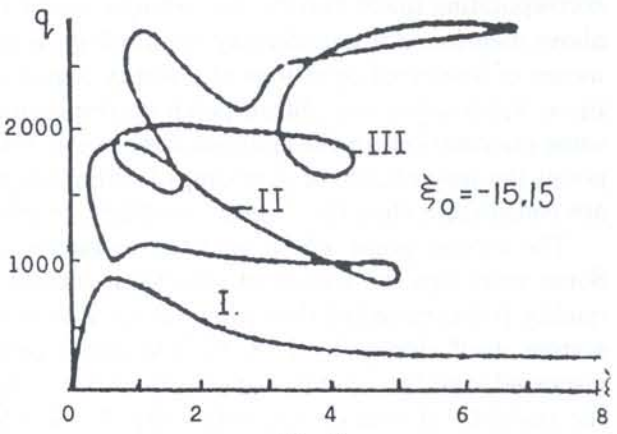

Fig. 6

In Figs. 3–6 case of clamped spherical segments which undergo external (acting from the outside) uniform pressure is presented, with dimensionless parameter q marked on the vertical axes. In these and in following figures, which describe the deformation of spherical caps, there are given the values of the initial geometrical parameter $\xi_0 = H/h$, where: H — initial height of the cap, h — its thickness, $\xi_0 < 0$ is for convex caps.

In Figs. 7 and 8 there are given corresponding deformation curves of spherical segments supported at the edge by hinges immovable in the radial direction and subjected to boundary bending

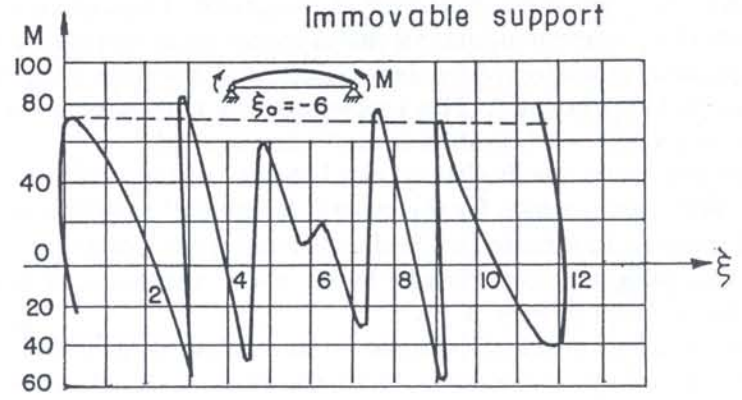

Fig. 7

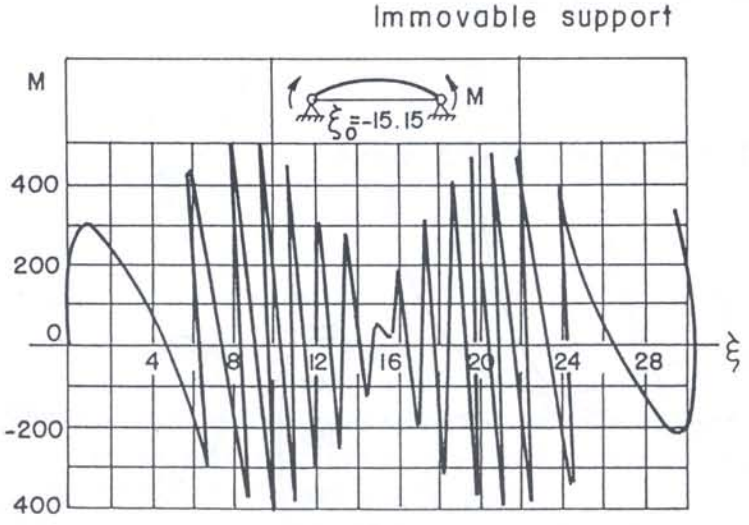

Fig. 8

moments uniformly distributed along this edge (axisymmetrical "pure bending") with the dimensionless parameter M marked along the vertical axis along the vertical axis. Figure 9 shows the case when the hinge supports are movable in the radial direction. In Fig. 10 the vertical axis is the axis of dimensionless parameter P of the central force [19].

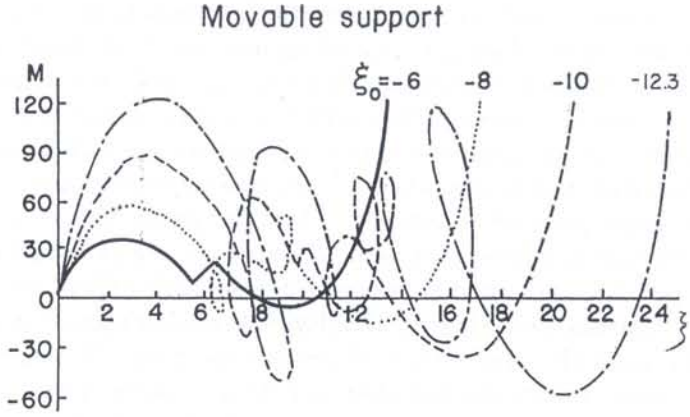

Fig. 9

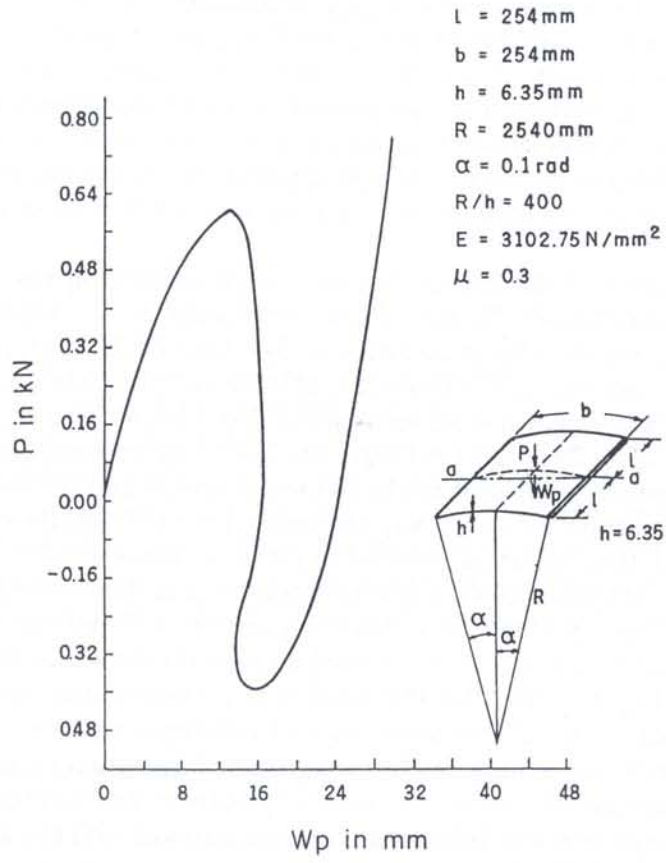

Fig. 10

All the above presented plane deformation curvers are projections of the corresponding real deformation paths in the infinite dimensional space. If there are no bifurcation points, then these curves contain (if they are complete) the complete information about all the possible equilibrium

states of the considered object for any value of the loading parameter. But even in such a simple case this curve is not a global picture of the investigated system since so far stability of all the possible equilibrium states has not been considered.

As it was explained in [18, 20, 21] there exist only two branches of each deformation curve in which there are stable equilibrium states. They are the left and right extremal branches as shown qualitatively in Fig. 2a, where points A and B are the first maximum and the last minimum respectively. This important feature does not depend on how many intermediate branches there are between the two stable ones shown. In case of spherical segments the number of mentioned intermediary (nonstable) branches increases together with an increase in the geometrical parameter $|\xi_0|$. Thus for each value of the loading parameter there can exist no more than two stable states in case of exisymmetrical deformation and it seems to be a universal feature of any geometrically nonlinear system subjected to a single parametric loading. Then the graph in Fig. 2a is in fact the global picture of stability if bifurcation points are absent. An example of a global picture of stability where secondary bifurcation points do not exist is famous Euler's elastic [22] which describes the bifurcation plane shapes of a compressed bar. In case of axisymmetrical deformation of shells of revolution, bifurcation phenomena mean the appearance of asymmetrical equilibrium forms adjacent to the critical axisymmetrical ones, despite the fact that all external conditions (loading, initial geometry, supports and features of the material) remain symmetrical. Thus the postbifurcation branches are of the type shown in Figs. 1 or 2b.

Absence of bifurcation points in case of spherical shallow caps, for example, takes place for small $|\xi_0|$ and edge supports which are immovable in the radial direction [18, 23]. But if these supports are movable, then (for any values of $|\xi_0|$) bifurcation points always exist. They are the so-called "bifurcation in tension", and the corresponding bifurcation points are located on the branches shown in Fig. 2a far from points A and B [18]. When $|\xi_0|$ is not very small, there also appear additional "bifurcations in compression". In general, new unstable branches of the corresponding deformation curves can correspond to bifurcation points. The number of such branches is infinite because the spectra of bifurcation values of the loading parameter are discrete and infinite. On each unstable branch new (secondary) bifurcation points can appear which are origins of new (additional) branches and so on.

Thus the global picture of the system behavior when bifurcation phenomena are taken into account is extremely complicated. To the author's knowledge the branches which are associated with the bifurcation points are almost investigated for shells of the type presented in the figures given above. There are only two publications [24, 25] that include investigation of a small element of the postbifurcation branch which emerges from the first (smallest) bifurcation value of the loading parameter in cases of shallow spherical segments loaded by external pressure and central bulk force. The element question is adjacent to the bifurcation point and the knowledge of its position (inclination) is very important for us to judge the sensitivity of the shell to the geometrical imperfections always existing. It is important if we are to judge the influence of these imperfections in the behavior of shell in the neighbourhood of a bifurcation point and the initial postbifurcation stage. The results of [24, 25] were realized by Koiter's asymptotical (local) method [15, 16]. Different, very complex, postbifurcation paths were obtained numerically for semispherical caps subjected to external pressure (see Fig. 11), [26]. But the stability of postbifurcation states was not considered in [26] nor in other sources. In [27] we find results of contemporary investigation of the distribution of bifurcation points (spectrum), of the emerged postbifurcation paths and stability of some postbifurcation paths in case of compressed circular cylindrical shells. Bifurcations in the last case mean transfer from axisymmetrical deformation to asymmetrical with the formation of waves both in circumferential and axial directions.

Thus the investigation of the global picture of stability is today only at very initial stage even in case of a single parametric external excitation. Of course, the situation is more complicated when the system of loadings is a multiparametric loading. This problem is considered in the next section. To finish this section, it is worthwhile to notice the following. There exists an opinion that it is not necessary to have the deformation curve in the postcritical stage, i.e. after loss of stability (by

bifurcation or by snap through), since real structures are designed on the criterion that the actual value of loading is smaller than the critical one. Such an ultra practical approach is not satisfactory because for really good (optimal) design it is necessary to have the scenario of possible behavior of the structure in general, because only thus we are able to rationally use the resources of the structure's strength while being at the same time more assured of its reliability. Briefly speaking,

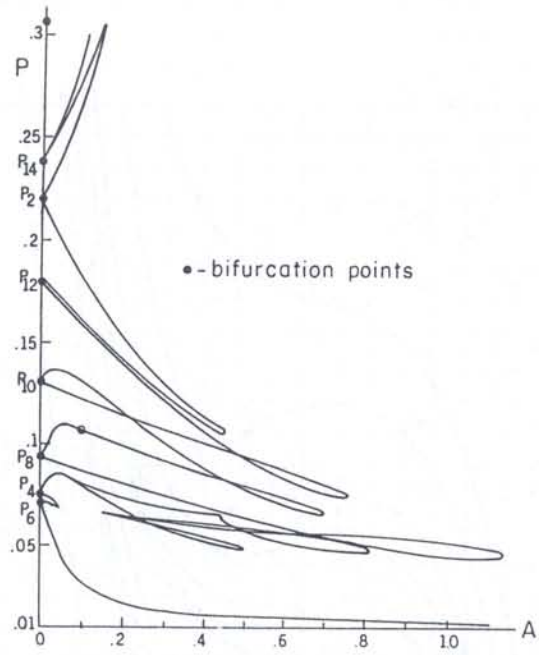

Fig. 11

it is necessary to know what can happen to the structure if stability is lost. Besides this, knowing the critical states, it is possible to avoid their formation by introducing additional elements which are usually called "stiffeners". But stiffeners are not the only obstacles to the formation of critical states by increasing the critical values of loading parameters, but also, for example, corrugation or corresponding changes of the boundary conditions (supports).

Thus, again, the revelation of critical states (including the postcritical ones, which appear during the secondary loss of stability, and so on) is very important for optimal design, or design in general, and not only of "academic interest". Unfortunately, this last expression is generally used in a contemptunous form. However, we must remember that todays pure scientific (academic) results is, as a rule, very practical tomorrow. The whole history of science and technology is a witness to such a continuous transformation. On the other hand, no theory exists which does not have an academic interest.

2. Multiparametric loading

As it has been mentioned above, this case is naturally much more complicated than the behavior under a single parametric loading. First of all we shall note the books [17, 28, 29] which consider local stability in the neighbourhood of bifurcation points of nonlinear systems of finite degrees of freedom subjected to multiparametric external excitations. In [30] the bifurcation problem of a circular plate subjected to transverse and compressing forces at the edge is investigated. In [31] the problem of bifurcation of axisymmetrical loaded spherical shells under three parametric loadings i.e. edge bending moments, transverse pressure and edge compressing forces, is investigated.

Concerning global stability, it can be said that attempts in this direction were undertaken by means of investigations of the behavior of different geometrically nonlinear shells and plates subjected to two (in a few cases to three) parametric loadings, but only for small ranges of these parameters values. See, for example, Figure 12 in which there is depicted a series of deformation curves $M(\xi)$ for different $q = \text{const}$ of a movable hinged supported spherical cap with $\xi_0 = -4$ which undergoes axisymmetrical deformations. Such deformation curves in Fig. 9, where $q = 0$ and ξ_0 takes different values.

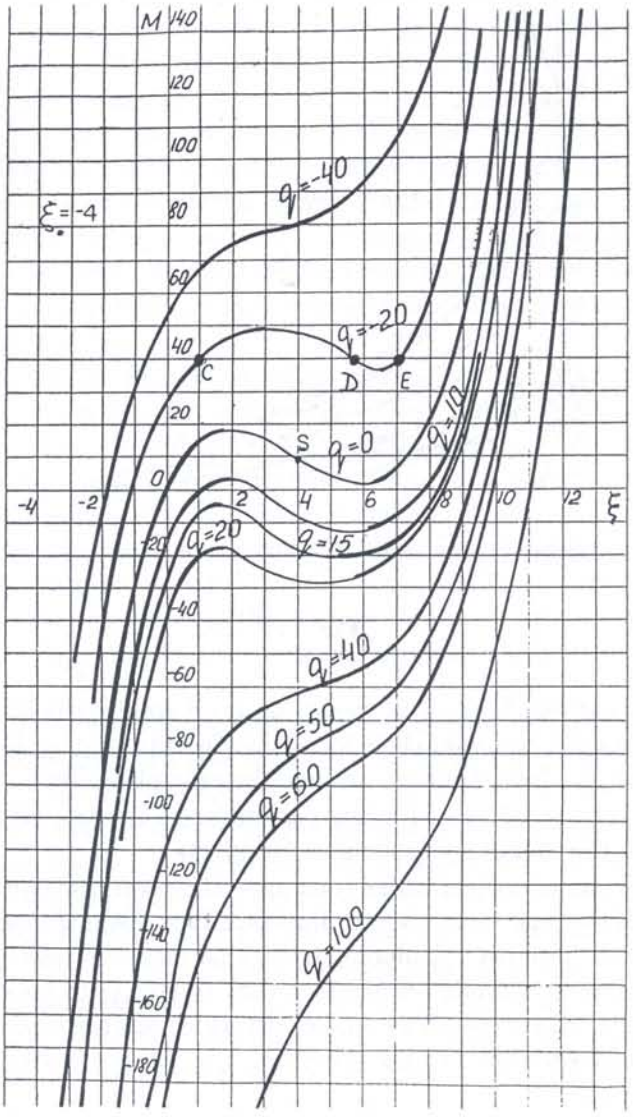

Fig. 12

In Fig. 12 stable branches are distinguished by black lines as in Fig. 2a, in accordance with the feature of existence of not more than two stable states for each value of the parameter of single parameter loading [18, 20, 21, 32]. It is interesting that when $|q|$ increases ($q > 0$ when the pressure is applied from the outside (convex) of the cap) the difference between the upper and lower critical values of M decreases and finally, beginning from $|q| \approx 30$–35, loss of stability by snap-through in the class of axisymmetrical deformations is avoided, i.e. the corresponding deformation curves $M(\xi)$ are monotonic.

The same effect takes place for deformation curves $q(\xi)$ for different values of edge moment M

(the curves $q(\xi)$, were obtained by projection of the family of curves from Fig. 12 into plane (ξ, q)). Thus the addition of M can avoid a snap-though process under the action of pressure q. Note also that this effect does not depend on the signs of q or M, and is not a trivial self-explanatory one because it is for shells and not only for plates. Applying multiparametric loading to the system we have considerably more possibilities of manoeuvring and controlling the system, and optimizing its behavior in conformity with previously given criteria.

Let us consider, for example, deformation curve $M(\xi)$ when $q = -20$ and observe the states which correspond to $M = 40$. There are three such states marked by C, D and E in Fig. 12. On the other hand when $q = 0$ and $M = 40$ we can easily see that for this loading there exists only a unique equilibrium state (see point A on the curve for $q = 0$ in Fig. 12). When $M = 0$ and $q = -20$, then we can see that again there is only one equilibrium state [18]. Thus the combination of two one parametric cases $q = 0$, $M = 40$ and $q = -20$, $M = 0$) brings us to a new situation, where for $q = -20$ and $M = 40$ there exist already three states. Thus multiparametric loading leads to new behavior and new features.

The picture presented in Fig. 12 is a global one if there are no bifurcations. There probably are no bifurcations in compression for $|\xi_0| = 4$ (see [18]), but bifurcation points in stretching exist and they are located on each deformation curve on both its monotonic branches, far from the central part of the curve. It is worthy of note that the central curve ($q = 0$) of the family of curves in Fig. 12 is of a screw symmetrical type with the center of symmetry in point S, shown in Fig. 12. The spectrum of bifurcation points in this case consists of pairs of points symmetrically located relative to S. When $q \neq 0$ the corresponding deformation curves are not symmetrically located. In case of immovable hinge supports families of curves similar to those presented in Fig. 12 are fully global pictures for all $|\xi_0| \leq \approx 1.5$ since then these are no bifurcation points, but limit points can appear [18].

Some attempts to consider cases of two parameter loadings were undertaken in [33] for spherical caps, in [34, 35] for cylindrical shells and others. But all these works, despite their high quality, do not deal systematically with global stability in the sense explained in the first part of the paper. "Deformation map" [36–38 and others of the author] which can be used for two and three parametric external excitations is a very convenient tool deal with such a global picture.

3. Deformation map

We shall proceed now to describe the so-called "deforamation map" for a geometrically nonlinear, linear elastic shallow shell of revolution which is rotationally orthotropic (the axes of the shell and orthotropy coincide) and undergo axisymmetrical thermoelastic deformations. This class of problem is very wide and is an example of a complicated nonlinear system which possesses an extremely rich complexity of essentially nonlinear features charcteristic of geometrically nonlinear systems in general. As is well known the diversity of behavior and richness of these systems are results of their symmetry, because they can posses both symmetrical and asymmetrical forms.

3.1. Basic equations of shallow caps

The basic equations of Karmann–Marguerre type for axisymmetrical deformations of geometrically non-linear, rotationally orthotropic, shallow caps (plates in particular) that take thermal stresses into account may be written in the form shown in equations (5) and (6) [39, 40, 42] below. The constitutive Hooke–Neumann law for an elastic material is given in the case, by equations (1) and (2):

$$\bar{\varepsilon} = \frac{\bar{\sigma}_r}{E_r} - \frac{\mu_\varphi}{E_\varphi}\bar{\sigma}_\varphi + \alpha_r T\,, \quad \bar{\varepsilon}_\varphi = -\frac{\mu_r}{E_r}\bar{\sigma}_r + \frac{\bar{\sigma}_\varphi}{E_\varphi}\bar{\sigma}_\varphi + \alpha_\varphi T\,, \tag{1}$$

$$E_r\mu_\varphi = E_\varphi\mu_r\,, \tag{2}$$

where: $\bar{\varepsilon}$, $\bar{\sigma}_r$ and $\bar{\sigma}_\varphi$ — components of deformations and stresses, respectively, in any layer at distance Z from middle surface, E_r, E_φ, μ_r, μ_φ and α_r, α_φ — Young's moduli, Poisson's ratios and thermal coefficients in meridional and circumferential directions, respectively, when the center of orthotropy coincides with the center of the middle surface. These parameters are taken to be independent of increment T of temperature field. T can be a function of Z and the dimensionless radial coordinate $\sigma = r/a$, where a is a the radius of the base of the cap.

For an arbitrary anisotropic body, the following inequality holds [41]:

$$\mu_r + \mu_\varphi + \mu_z \leq 3/2\,. \tag{3}$$

If we take into account Kirchhoff–Love hypothesis of incompressibility of the shell in Z direction, inequality (3) reduces to equation (4)

$$\mu_r + \mu_\varphi \leq 1\,. \tag{4}$$

$$L_k(\omega) = k2\left[-\frac{\theta^2 + 2\theta\theta_0}{2\rho}\frac{a^2}{h^2}\left(\frac{1-\lambda^2}{\rho}N_T - \lambda^2 N_T'\right)\right], \tag{5}$$

$$L_k(\theta) = -m_\alpha\left[\frac{1}{\rho}\int_0^\rho \rho q(\rho)\,\mathrm{d}\rho + \frac{P}{\rho} - \frac{\omega(\theta+\theta_0)}{\rho}\right]$$
$$+\frac{12a^2}{h^2}\left[\frac{(1-k^2\mu_r) - k^2\lambda^2(1-\mu_r)}{\rho}M_T + (1+\mu_r k^2\lambda^2)M_T'\right], \quad (0 \leq \rho \leq 1)\,. \tag{6}$$

These equations are true for cap-shaped shells with no hole at the apex. All the parameters are given in dimensionless form:

$$k^2 = E_\varphi/E_r\,, \quad \lambda^2 = \alpha_\varphi/\alpha_r\,, \quad m_\alpha = 12(1-\mu_r\mu_\varphi) = 12(1-\mu_r^2k^2)\,, \tag{7}$$

$$N_T = \alpha_r\int_{-1/2}^{1/2} T(\rho,\zeta)\,\mathrm{d}\zeta\,, \quad M_T = \alpha_r\int_{-1/2}^{1/2}(\rho,\zeta)\,\mathrm{d}\zeta\,, \quad \zeta = z/h\,, \tag{8}$$

where h is the thickness of the shell wall. Operator L_k is:

$$L_k(\,) = \frac{\mathrm{d}^2(\,)}{\mathrm{d}\rho^2} + \frac{1}{\rho}\frac{\mathrm{d}(\,)}{\mathrm{d}r} - k^2\frac{(\,)}{\rho^2}\,. \tag{9}$$

The unknown variables are the membrane stress function $\omega(\rho)$ and the angle of revolution $\theta(\rho)$ of the normal to middle surface. All the parameters of the problem are expressed by these functions, as shown below. In the relationship referred to below the dimensional (physical) quantities are denoted by asterisks.

The normal membrane forces, membrane stresses, elongations of the middle surface, increments of curvatures of this surface and bending moments are expressed in terms $\omega(\rho)$, $\theta(\rho)$ and $T(\rho,0)$, by the following formulae:

$$N_r(\rho) = N_r^*(\rho)a^2/E_rh^3 = \omega(\rho)/\rho\,, \quad N_\varphi(\rho) = N_\varphi^*(\rho)a^2/E_rh^3 = \omega'(\rho)/\rho\,; \tag{10}$$

$$\sigma_r(\rho) = \sigma_r^*(\rho)a^2/E_rh^2 = \frac{\omega(\rho)}{\rho} + \frac{a^2}{h^2}\frac{1+\mu_rk^2\lambda^2}{1-k^2\mu_r^2}[N_T - \alpha_rT(\rho,0)]\,. \tag{11}$$

$$\sigma_\varphi(\rho) = \sigma_\varphi^*(\rho)a^2/E_rh^2 = \omega'(\rho) + \frac{a^2}{h^2}\frac{k^2(\lambda^2+\mu_r)}{1-k^2\mu_r^2}[N_T - \alpha_rT(\rho,0)]\,; \tag{12}$$

$$\varepsilon_r(\rho) = \frac{h^2}{a^2}\left[\frac{\omega(\rho)}{\rho} - \mu_r\omega'(\rho)\right] + N_T(\rho)\,;$$

$$\varepsilon_\varphi = \frac{h^2}{a^2k^2}\left[\omega^2(\rho) - \mu_r k^2 \frac{\omega(\rho)}{\rho}\right] + \lambda^2 N_T(\rho)\,; \tag{13}$$

$$\chi_r(\rho) = \chi_r^*(\rho)a^2/h = \theta'(\rho)\,, \quad \chi_\varphi^*(\rho)a^2/h = \theta(\rho)/\rho\,; \tag{14}$$

$$M_r(\rho) = M_r^*(\rho)a^2/D_r h = \theta'(\rho) + \mu_r k^2\theta(\rho)/\rho - \frac{12a^2}{h^2}(1 + k^2\mu_r\lambda^2)M_T(\rho)\,,$$

$$M_\varphi(\rho) = M_\varphi^*(\rho)a^2/D_r h = k^2[\theta(\rho)/\rho + \mu_r\theta'(\rho)] - \frac{12a^2k^2}{h^2}(\lambda^2 + \mu_r)M_T(\rho)\,. \tag{15}$$

where: $D_r = E_r h^3[12(1-\mu_r^2k^2)]$.

The bending moments are positive if they influence the increasing the curvatures of the middle surface. The curvature of the meridian is positive when the convexity of the shell is directed downwards in the positive direction of Z-axis. The horizontal and vertical displacements of the points on the middle surface are:

$$u(\rho) = u^*(\rho)/h = \rho\varepsilon(\rho)a/h = \frac{\rho h}{ak^2}\left[\omega'(\rho) - \mu_r k^2\frac{\omega(\rho)}{\rho}\right] + a\lambda^2\rho N_T(\rho)/h\,. \tag{16}$$

$$w(\rho) = w^*(\rho)/h = -\int_0^\rho \theta\,\mathrm{d}\rho + \xi\,, \quad \xi = w(0)\,. \tag{17}$$

If the boundary points are fixed, then:

$$w(\rho) = \int_\rho^1 \theta\,\mathrm{d}\rho \quad \text{and} \quad \xi = \int_0^1 \theta\,\mathrm{d}\rho\,, \tag{18}$$

where u is positive in the direction away from the apex, w is positive in the direction of Z-axis and is measured from the underformed (original) meridian. The shape of the underformed meridian is represented by function $w_0(\rho)$ that is physically identical to function $w(\rho)$ and parameters ξ_0 are positive when the convexity of the underformed shell is directed downwards.

The distributed and concentrated loads, are positive if they are directed downwards and they can be expressed by the relationships:

$$q(\rho) = q^*(\rho)a^4/E_r h^4\,, \quad P = P^*a^2/2\pi E_r h^4\,. \tag{19}$$

The most frequently used boundary conditions can be written in the form:

$$\omega(0) = \theta(0)\,, \quad \alpha_1\omega'(1) + \beta_1\omega(1) = \gamma_1\,, \quad \alpha_2\theta'(1) + \beta_2\theta(1) = \gamma_2\,. \tag{20}$$

The conditions at $\rho = 0$ ensure continuity and boudness of functions ω, θ in the vicinity of the apex. Condition at $\rho = 1$ for ω characterizes the degree of mobility of boundary supports in the plane of shell base. The last relationship (20) characterizes the type of support affecting the bending conditions at the boundary. Two conditions (20) at $\rho = 1$ are in general independent to each other. Nine basic combinations of boundary conditions are given in Table 1.

Table 1. Nine basic combinations of boundary conditions

	Mobile support without normal boundary forces	Mobile support with active normal boundary force N	Immovable support
Conditions for ω	$\alpha_1 = 0,\ \beta_1 = 1,\ \gamma_1 = 0$	$\alpha_1 = 0,\ \beta_1 = 1,\ \gamma_1 = N$	$\alpha_1 = 0,\ \beta_1 = -\mu_r k^2$ $\gamma_1 = -a^2k^2\lambda^2 N_T(1)/h^2$
Conditions for θ	$\alpha_2 = 0,\ \beta_2 = 1,\ \gamma_2 = 0$	$\alpha_2 = 1,\ \beta_2 = \mu_r k^2,$ $\gamma_2 = \frac{12a^2}{h^2}(1+k^2\lambda^2\mu_r)M_T(1)$	$\alpha_1 = 1,\ \beta_1 = \mu_r k^2$ $\gamma_2 = M + \frac{12a^2}{h^2}(1+k^2\lambda^2\mu_r)M_T(1)$
	Clamping	Hinged support without boundary bending moment	Hinged support with bending moment M

3.2. Deformation maps for nonlinear plates

Let us now some examples of deformation maps and their application. Some examples of deformation maps are given in Figs. 13 and 14 for $k = 0.5$ and 1, respectively, when the transversal conditions. forces are $q = P = 0$ and there are no thermal stresses. The support is of a movable

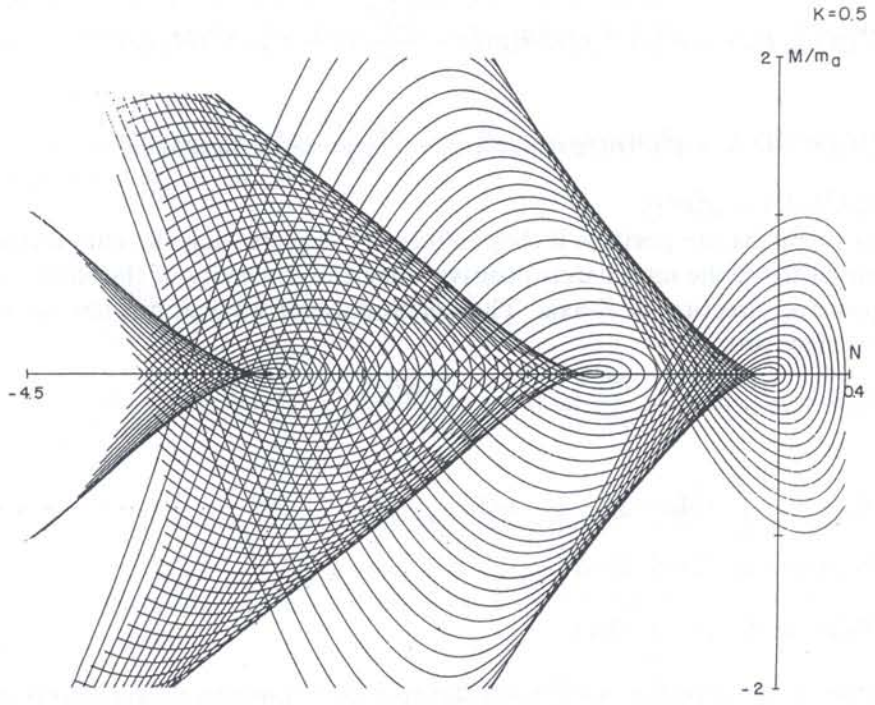

Fig. 13

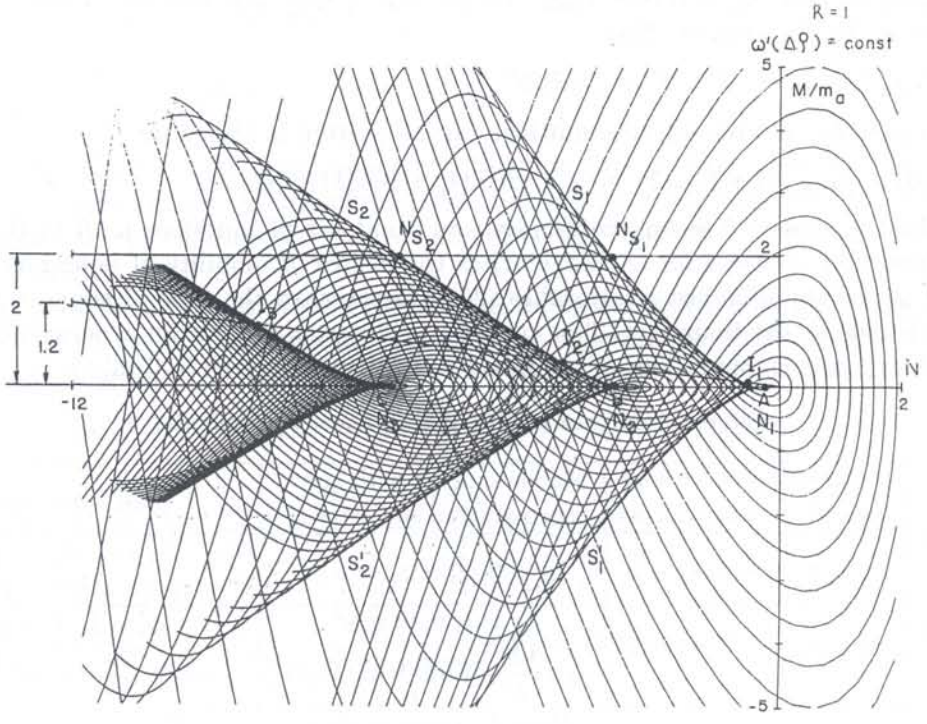

Fig. 14

hinged type. The same qualitative shapes have their corresponding maps for any $k < 1$ or $k > 1$ in the above-mentioned

The deformation maps are built in N, M/m_α plane by means of corresponding solutions of Cauchy's problem. Since the system of basic equations (5) and (6) are of fourth order, four initial conditions are needed to solve Cauchy's problem. To work out these conditions we use Property 1 from [42] which shows that in the vicinity of initial point $\rho = 0$ the unknown functions $\omega(\rho)$, $\theta(\rho)$ are of $A\rho^k$ order. Consequently, we can write for any $\Delta\rho \ll 1$:

$$\omega(\Delta\rho) = \omega'(\Delta\rho)\Delta\rho/k\,, \quad \theta(\Delta\rho) = \theta'(\Delta\rho)/k\,, \quad (0 < \Delta\rho \ll 1)\,. \tag{21}$$

If we now set values of $\omega'(\Delta\rho)$, $\theta'(\Delta\rho)$ and find $\omega(\Delta\rho)$, $\theta(\Delta\rho)$ from equation (21), then the solution to the corresponding Cauchy's problem may be obtained by means of any numerical method, for example by Runge–Kutta method. Thus, we can calculate boundary N and M which correspond to these predefined initial conditions. By calculating parameters N and M in this manner we can determinate a certain point on the deformation map built in (N, M) plane. Each curve in this plane (represented in Figs. 13 and 14) will correspond to a value of $\omega'(\Delta\rho)$. Consequently, the map is really a single-parameter family of curves with parameter $\omega'(\Delta\rho)$. This family of curves provides a lot of information on the plate's bahaviour under loading.

We may notice in Figs. 13 and 14 that on the N axis there are some singular points which are denoted A, B, C, ... These points provide the values of classical critical loads N when planar forms change to axisymmetrical bent forms. The first three critical loads are presented in [42] in dimensionless form for: $k = 0.5$, 1.2.

All numerical solutions described in the paper are computed for $\mu_r = 0.3$ and the corresponding ratio is $\mu_\varphi = \mu_r k^2$. The values of critical N for classic case ($K = 1$, $\mu = 0.3$) correspond to the known solutions (see, for example [22]).

A pair of rays situated symmetrically relative to N axis comes from each of the above-mentioned irregular points A, B, C, ... These rays, which are denoted in Fig. 14 by S_1, S_1'; S_2, S_2; S_3, S_3' ..., respectively, divide (N, M) plane into regions of different topological structure. Only one curve of deformation map passes through each point of the region situated outside the angle formed by rays S_1 and, S_1'. This means that for N and N_1 corresponding to these points only one unique state of plate can exist (only one solution of the basic equation). In the region between the pairs of rays S_1, S_1' and S_2, S_2' three curves pass through each point. Thus, three corresponding states of plate exist. Between the pairs of rays S_2, S_2' and S_3, S_3' there are five solutions for each pair of values N and M.

The topological structure of deformation map opens up the possibility of studying the behavior of plate under the conditions for which the map was constructed. The deformation map, which similar to the well known Poincaré phase plane of autonomous dynamic systems, contains in a concentrated form all the qualitative and quantitative information on the behavior of this plate, loaded by two parametric systems of forces N and M. Or, to be more exact, there is volume of information that may be obtained from the considered boundary problems of the system of equations (5) and (6).

Suppose, for example, we want to know the behavior of the plate for various values of M when N is fixed. If $N > N_1$ then for arbitrary value of M there is only one unique equilibrium state because vertical $N = \text{const.} > N_1$ passes outside the region of S_1, S_1' angle. Now, let us assume that vertical $N_1 = \text{const.}$ is situated between N_1 and N_2. Then a part of this vertical passes through the region of S_1, S_1' angle, where for each pair of values of N and M there are three solutions of the basic equations. Outside the S_1, S_1' angle this vertical passes through the field where for any pair of N and M there is only one unique equilibrium state. Then, when $N_2 > N = \text{fixed} < N_1$ and M varies, there may be a loss of stability by snapping. The corresponding upper (lower) critical value of M is the ordinate of the point of intersection the above-mentioned line $N = \text{const.}$ and $S_1(S_1')$ curve. The upper and lower critical values of M are equal but they have opposite signs because of the symmetry of the map relative to the horizontal axis.

When vertical N lies between N_2 and N_3, it passes in part through both regions inside the angles between S_1, S_1' and S_2, S_2'. Then the greatest number of solutions of basic equations (5) and (6)

is five. But the critical values of M are also the ordinates of points of intersection of S_1, S_1' curves and the line $N = \text{const.}$ since the angle S_2, S_2' is smaller than S_1, S_1'. The same situation is seen in the interval $N_4 < N < N_3$ with the number of solutions increased by two, and so forth.

Consequently, curves S_1 and S_1' are graphs of the dependence of N on the upper and lower critical values of M, respectively. Thus we observe that for increasing values of $|N|$, where N is compressive, the upper critical moment M increases and vice versa for the lower critical values of M. We also see that the classically critical values of N take on and additional meaning. They are also, at the same time, the values of N when the number of solutions of the basic boundary problem examined here is changed to two. N_1 is the value N associated with the start of the snapping process under moment M when $N = \text{const.}$

These properties of plates are confirmed by numerical solutions for specific cases shown in Fig. 15. They represent the so-called "characteristics" of the plate (the graphs of functions $M(\xi)$) for various values of fixed N and $k = 0.5$ (only halves of the graphs were drawn since Fig. 15 is symmetrical with respect to the origin). In this figure two monotonous curves are built for $N > 0$ and $0 > N > N_1$ and two other curves are constructed for $N_2 < N < N_1$ and $N_3 < N < N_2$. The same shapes are the characteristics for any $k > 0$.

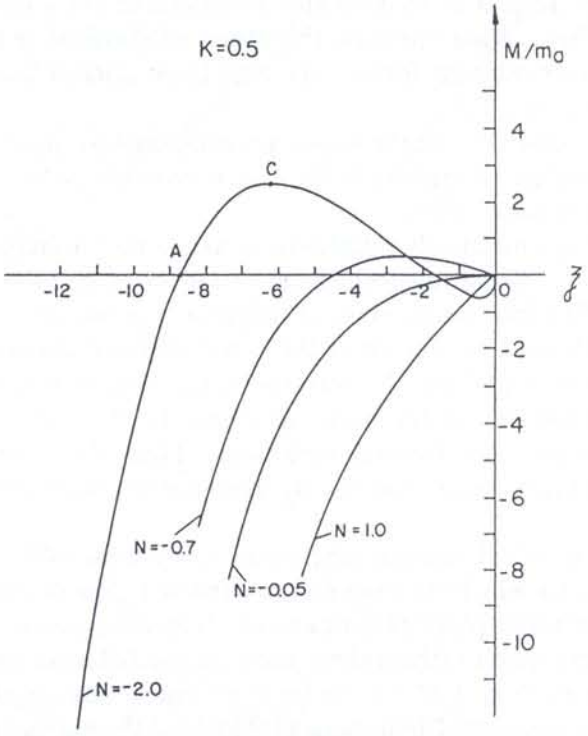

Fig. 15

The above-mentioned loss of plate stability by snapping may be explained in the light of an example when $k = 0.5$ and $N = -2$ (see Fig. 15). When $M = 0$ the plate may be in two opposite symmetrical states with $\xi = \pm 8.7$ (point A in Fig. 15 and corresponding symmetrical points). When the moment increases from the initial state on the plate for $\xi = 8.7$, loss of stability is impossible because the part of characteristic curve $M(\xi)$ beyond point ($\xi = 8.7$, $M = 0$) is monotonous. If we start from point ($\xi = -8.7$) in the positive direction M, then loss of stability by snapping will occur at point C. In the latter case, positive bending moment M acts on the convex side of the plate deformed by force $N = -2$ and, thus loss of stability may occur. In the former case, an opposite situation is seen and the phenomenon of snapping cannot occur.

Now let us investigate the intersections between the deformation map and horizontal lines. Line

$M = 0$ describes the behavior of plate under action of N. When $N > N_1$, the plate is in the critical or post-critical state of equilibrium. All these phenomena are well known (see for example [43] and others). The corresponding characteristics have the shape shown in Fig. 16. A transition through any bifurcation point N_i changes the number of corresponding solutions for the basic equation by

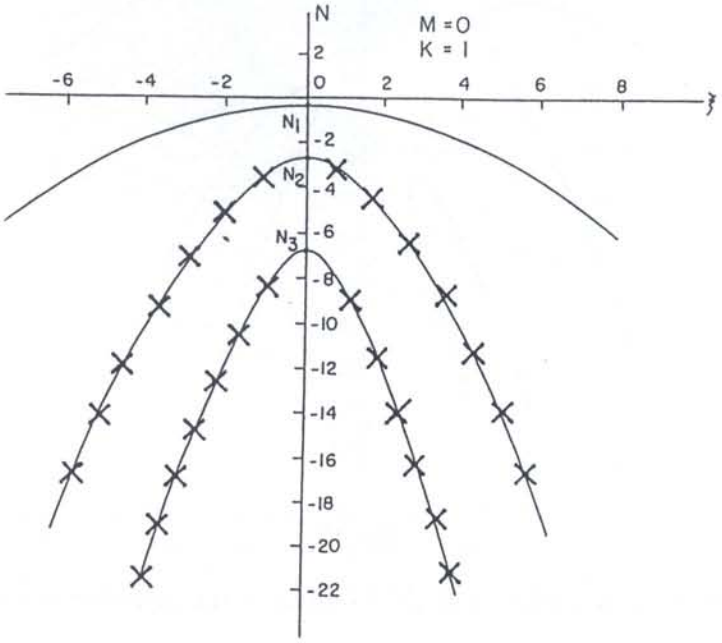

Fig. 16

two. Line $M = \text{const.} \neq 0$ provides the following information. For $N > N_{S1}$ (where N_{S1} is the intersection point between line $M = \text{const.}$ and curve S_1) there is only one unique state of plate (see, for example, Fig. 14). From inequalities $N_{S1} < N < N_{S1}$ there are already three solutions for the basic equations, etc. The shape of the characteristics is shown in Fig. 17 for $M = 2m_\alpha$; the support is of a movable hinged type. To obtain the characteristics for $M < 0$, we must invert characteristics for $M > 0$ which is symmetrical relative to N axis. Therefore, if $M \neq 0$ bifurcation phenomena of the type for which $M = 0$ do not exist. A continuous transition from the monotonous branch of the characteristic (see Fig. 17) to the other branches is impossible. This transition may be realized only if an additional specific impulse is applied. As a result, the addition of moment M in fact eliminates the danger of plate loss of stability which is usually caused by action of N.

Let us now look at the influence of eccentricity of compressive force N on its own critical values. In this case the boundary conditions may be written in the form:

$$M = eN\,, \tag{22}$$

where eccentricity $e > 0$ when force N is situated under plate and $e < 0$ in the opposite case.

To investigate this important problem, we must examine the intersections of the lines (22) with deformation map. Let us take, for example, case $e > 0$. Points of intersections of line $M = eN$ and curves S_1, S_2, ... of the deformation map are denoted as I_1, I_2, ... (see, for example, Fig. 14). Then the part of the line situated between the point of origin of the map and the point I_1 lies in the region of the map where there a unique equilibrium state of plate for each value of M or N. For values of M larger than ordinate of I_1, the above-mentioned line enters the field of the map where there are already three equilibrium states for each M. Above the intersection of the line (22) with curve S_2 there are five solutions and so on. The specific case in which $k = 1$ and $e = -0.1m_\alpha$ and the support is of the movable hinged type is similar in its qualitative properties to the case in which $M = \text{const.}$ (see Fig. 17). It differs, in principle, from the case of the compressed perfect bar.

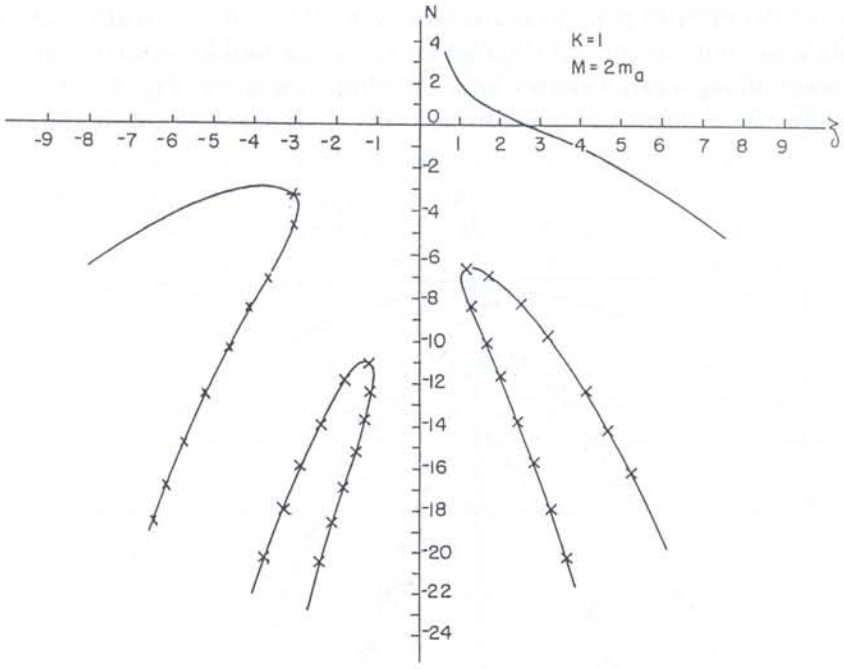

Fig. 17

But it may be said that the behavior of plate is similar to the behavior of a compressed bar with imperfections.

In the same manner we may investigate the behavior of plate under any loading. It is sufficient then study the intersection of loading path $F(M, N) = 0$ with curves $(S_1,\ S_1')$. For example using quasistatistical approach we can study the behavior of plate during fatigue process when $M = \text{const.}$ and N varies within limits $\pm\bar{N}$. Then, if line $-N \leq N \leq \bar{N}$ and $M = \text{const.}$ lies in the region outside angle S_1AS_1', the fatigue process is not accompanied by stability loss phenomena. In a contrary case, the straight and reverse snapping may occur at each cycle of loading and this fact must be taken into account during design.

On the other hand, the map is a store of quantitative information on the behavior of plate and may be used as a nomograph. For each point of loading path $F(M, N) = 0$ we can find from the map the initial parameters $\omega'(\Delta\rho)$ and $\theta'(\Delta\rho)$ with result from (21) of all equilibrium states corresponding to this point. It is often convenient to use, apart from the described map, the other variant based on the family of curves $\theta' = (\Delta\rho) = \text{const.}$ On the basis of the parameters all the characteristics of the considered equilibrium states may be easily found by numerical solution of the corresponding Cauchy problems.

3.3. Thermoelastic deformation of circular plates

Let us take a more complicated case, for example, thermoelastic deformation where the temperature field is isotropic ($\lambda = 1$), temperature T is an even function of Z and does not depend on ρ, the support is an immovable hinge, external force is $q = 30$, and $k = 0.5$. Thus, in this case $N_T(\rho) \equiv \text{const.}$ and $M_T(\rho) \equiv 0$ (see Eq.8). The corresponding deformation map is shown in Fig. 18, where the vertical axis indicated values of M/m_α and the horizontal axis indicates the values of the corresponding value of parameter γ_1 (see Table 1). The singular points of type A, B, C, ..., which exist in case when $q = 0$, (see Fig. 14) are not available now. For $q = 30$ there are essential topological changes of the map. For example, there is a region (noted by R on Fig. 18) where for all values of γ_1 and M only a unique equilibrium state of the plate exists. Above and below region R there are fields where more than one equilibrium state for each pair values of γ_1 and M exists. This

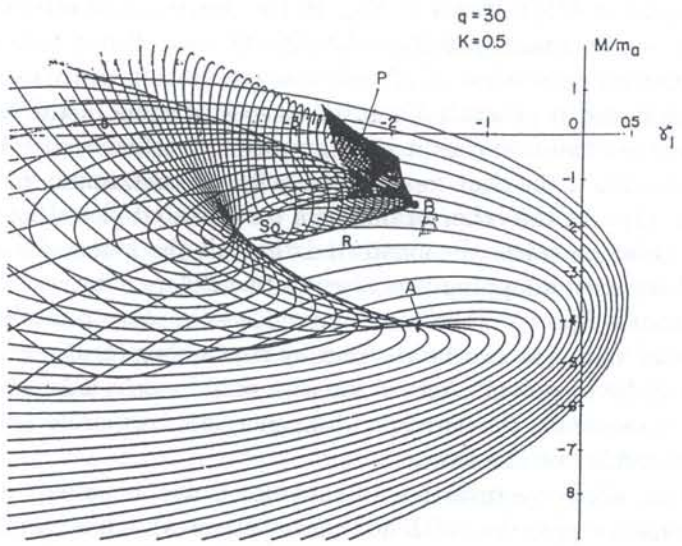

Fig. 18

fact causes the appearance of an isolated closed loop on graph $M(\xi)$ when $\gamma_1 = \text{const.}$ is fixed and line γ_1 crosses region R (ξ is the displacement of plate's center). Such graphs for different γ_1 which were drawn on the basis of numerical information from the map in Fig. 18 are given in Fig. 19.

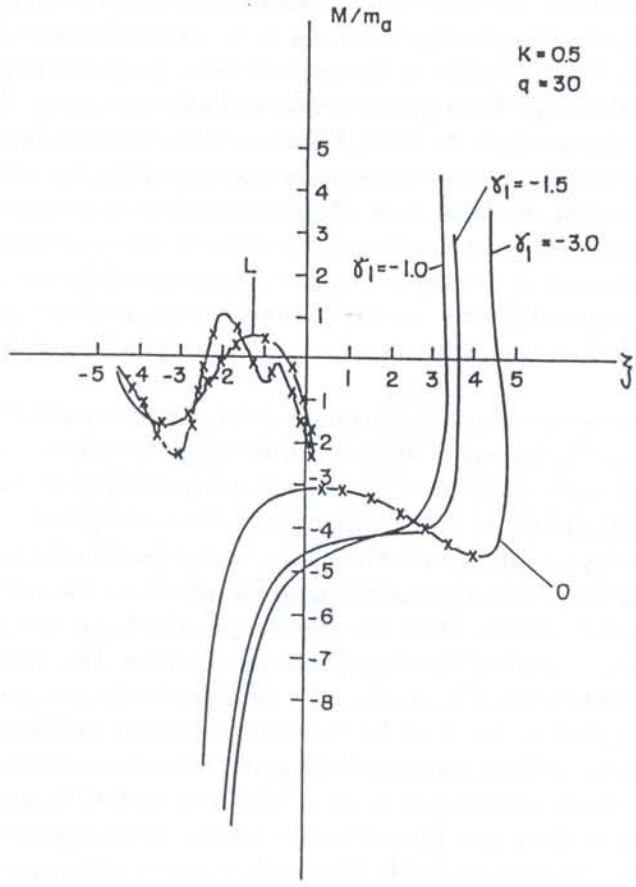

Fig. 19

From the three graphs of $M(\xi)$ drawn in Fig. 19 the dynamics of alteration in the behavior of plate when value of $\gamma_1 = 0$ decreases (fixed $q = 30$) can be seen. When $\gamma_1 > 1.5$ all the equilibrium states are stable because for each value of M only one equilibrium state exists. For $\gamma_1 < -1.5$ this uniqueness is distributed and it generated a stability loss of some of the equilibrium states. It is characteristic that there are two branches in each graph $M(\xi)$ when $\gamma_1 < -1.5$ (see graph $M(\xi)$ for $\gamma_1 = -3.0$). One of these has a classical "open" form with one maximum and one minimum (which is marked by 0 in Fig. 19) and the other branch is a complicated closed loop L. Our investigation of the stability of equilibrium states demonstrated that all the states denoted by "x" in Fig. 19 are unstable. Thus, there exist snapping processes of two different types. Snapping from one part of open branch 0 to another part on the same curve, or snapping to a stable part of loop L can occur. If the first type of snapping can be realized by continuous change of M, the second type of snapping can occur only by means of intervention of a certain external factor. The latter makes it possible for the plate to overcome the corresponding energetic barrier by transitions from a part of the "open" line to the stable one the loop.

In some of our earlier works we investigated cases for isotropic spherical shells with a clamped support loaded by a constant pressure (with no thermal stresses), where similar loops were obtained (see Fig. 6). We found that all the equilibrium states corresponding to the points of the loops were unstable [20, 32] contrary to the aforementioned case.

3.4. Advantages of the nonlinear analysis by means of deformation maps

Let us consider the features and the quality of the map in general. The described deformation map is not the only one possible. Maps can be built on the basis of independent initial parameters and not only on the base of initial parameters $\omega'(\Delta\rho)$ and $\theta'(\Delta\rho)$ $(0 < \Delta\rho \ll 1)$ used. But the gist of the matter remains the same. The topological character of the map in invariant (not depending on the chosen initial parameters) because it is, a characteristic of the considered system (in the given conditions). The behavior of the system for a given loading path is defined by the corresponding section of the map. Then specific numerical solution can be obtained directly without using incremental methods inevitable in FEM, FDM, or other similar algorithms which are always associated with many cycles of iterative procedures and accumulation of numerical errors with a weak convergence near critical, singular point. The map enables us to utilize the Cauchy problem, which has a unique solution, whereas the boundary value problem of nonlinear systems has, as a rule, many solutions. This is an extremely important advantage of the use of deformation map. By means of this approach, many different cases of various nonlinear shells and plates for a variety of loading systems and boundary conditions can be investigated including, for example, the range of plasticity.

Deformation maps enable us to investigate qualitatively and numerically all the nonlinear structures that can be described by means of ordinary differential equations. They may also be used as nomographs for design of such structures. At present the possibility of constructing similar maps for cases described by partial differential equations is being investigated.

Finally, it seems to be interesting to note the liaison of the described map technique with the well know "shooting" method which was successfully used for numerical solution of equations of type (5) and (6) (see [18, 45, 46] and others). Both the shooting method and the map technique described are built on the same basis — that of Cauchy's problem solutions. The difference between these two approaches is as follows. When shooting method for numerical solution of a given specific boundary conditions problem is applied all the Cauchy (initial conditions) problem solutions which do not satisfy (with the previously defined precision) the given boundary conditions are rejected. In the map technique, contrary to the shooting method, all this very useful, formerly rejected, information is preserved and included in the maps. It can then be used to form a general picture of the behavior of the considered systems. It is understable that such a general diagram, which is a deformation map, needs more computer time than the numerical solution of a specific boundary conditions problem by the shooting or other numerical methods, but the purpose justifies the expense.

Now a very important question naturally arises. To what degree can be above given deformation maps represent the global picture of stability? We shall examine this question using the map presented in Fig. 14. This map can be a global one only for the axisymmetrical deformations for which it is built. Then lines S_1 and S_1', which emerge from the first singular point A, are the boundaries of the stability area of plate's axisymmetrical equilibrium states. The region of the map inside S_1AS_1' is unstable since through each point of this region more than one line of the family of lines on which the map is based pass. Thus for axisymmetrical deformation the map is global. In case of a mobile support, as was previously mentioned, there exists bifurcation in tension and than, in a general case line S_1AS_1' is a not more the stability boundary. In this general case the full boundary of stability can be established in the following manner. The values of N at singular (cups) points A, B, C, ... are, as mentioned before, classical critical (bifurcation) loading values of loss of stability of uniformly compressed circular plates ($M = 0$) when the bifurcation modes are axisymmetrical [22]. But there exists another discrete infinite spectrum of critical values of N when the bifurcation modes are asymmetrical. The corresponding nondimensional critical $|N|$ shall be labeled by α_1, α_2, ... For example, in isotropic case there are $\alpha_1 = 1.22$, $\alpha_2 = 2.32$, ... when $= 0.3$ [22], (the corresponding physical values of N are $N_1^* = -13.36D$, and $N_2^* = -25.08D/a^2$). Both points α_1, $\alpha_2$lie between A and B (Fig. 14). Thus distributions of critical values for axisymmetrical and symmetrical buckling are not of a regular structure when each critical point for axisymmetrical buckling is followed by a (corresponding) asymmetrical critical point.

It is worth noting that the term α_n of the discrete spectrum of bifurcation loading corresponds to asymmetrical buckling with n waves in the circumferential direction without knot circles (expect the contour of the plate). On the other hand, the magnitude of the lower bifurcation value of dimensionless is $M = M^*/12(1 - 2)a^2$ (where M^* is the physical value). It correspond to an asymmetrical form adjacent to the existing symmetrical form, e.g. in the case if $N = 0$ is known. (Of course loading continues to be axisymmetrical). This value of M is equal to ± 318 when $n = 4$ and 7 (see [18]). At this value M bifurcation in "tension" occurs, that is when the meridian of plate is stretched. The corresponding points on the map will be $N = 0$ and $M/m = \pm 19,121$. It is clear that the lower values of bifurcation moment M will increase when N increases.

Thus it is expected that there exist two rays P^+ and P^- which emerge from point α_1 and which are graphs of the dependence of the lower bifurcation values of M upon force N (see qualitative picture in Fig. 20). Then the boundaries of the zone of stability are rays P^+ and P^- which emerge

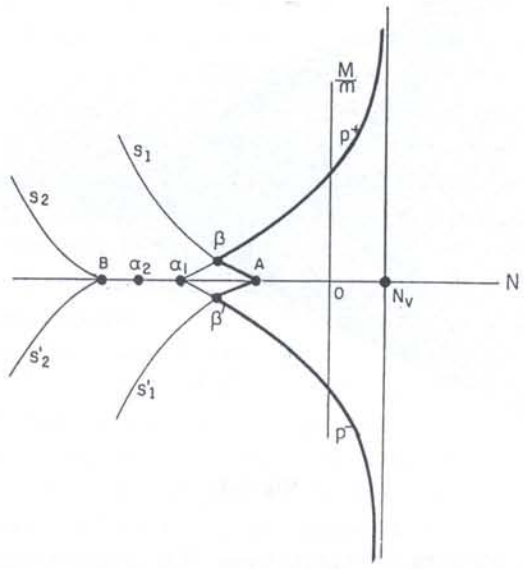

Fig. 20

from points β and β' , respectively (see Fig. 20 where β, β' are points of intersections of curves S_A, S'_a with P^+ and P^-) and lines $A\beta$ and $A\beta'$. The boundaries are shown in Fig. 20 by thick black lines. It is necessary to note that rays P^+ and P^- have a common vertical asymptote $N = N_V > 0$. That is, in general bifurcation points do not exist for any $N > N_V$, as was proved in [36]. The zone of stability will be the inside field bounded by "polygon" $P^+\beta A\beta' P^-$. A unique curve passes through each point of this area of the map and, in consequence, there is only a unique corresponding equilibrium state. Inside the angles $S_A\beta P^+$ and $S_A\beta' P^-$ one curve representing axisymmetrical equilibrium state and evidently other curves related to asymmetrical equilibrium are passing through each point. The curves P^+ and P^- are probable envelopes for the above mentionuos curves for different n.

The investigations are the first step, as far as we know, towards the solution of the problem of stability zones boundaries of geometrically nonlinear systems. It is expected that the main characteristic of the boundary will be preserved. It should also be true in more complicated cases of geometrically nonlinear plate and shells of revolution, loaded axisymmetrically. In any case, the boundaries considered show that the theorem of convexity of stability zones boundaries valid for linear cases (see [47]) is not confirmed in non-linear cases.

3.5. Three parametric loads of a circular plate

We shall now consider cases of three parametric external excitations. It is obvious the because the map is a two-dimensional (plane) figure, for the three-parametric loading it is necessary to have a one-parametric family of deformation maps. For example, if pressure q is acting (Fig. 14) then there will arise a family of deformation maps each of which is built for a fixed value of q. (Of course this is not the unique possibility. It can be taken as a parameter of the family of maps, each parameter of which is independent of the other two). An example of such a series of maps is given in Figs. 21, 18, 22–28 which describe the behavior of a circular, orthotropic plate. Each map is formulated for a corresponding constant value of q which is marked in each figure. On the vertical axes M/m_α are shown and on the horizontal axes — parameter γ_1 which is:

$$\gamma_1 = \omega'(1) - \mu_r k^2 \omega(1)\,. \tag{23}$$

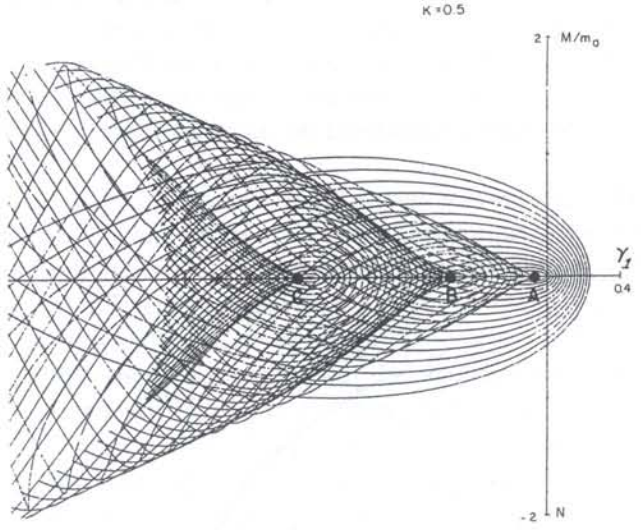

Fig. 21

This condition can have two different interpretations. If it is considered as a purely elastic problem (thermal stresses are omitted) then (23) has a physical meaning only when $\gamma_1 = 0$. The latter describes the case of immovable hinge support where dimensionless horizontal displacement $u(1) =$

$\omega'(1) - \mu_r \kappa^2 \omega(1) = 0$, and then only vertical section $\gamma_1 = 0$ of the maps are of interest. All such sections lie in the areas of maps where there only solution for each combination of M and $q(\gamma_1 = 0)$. In consequence, the plate which is supported by immovable hinge supports and subjected to two-parametric loading (M, q) always has only one unique equilibrium state. Bifurcations do not exist in this case because of the immovability of the supports.

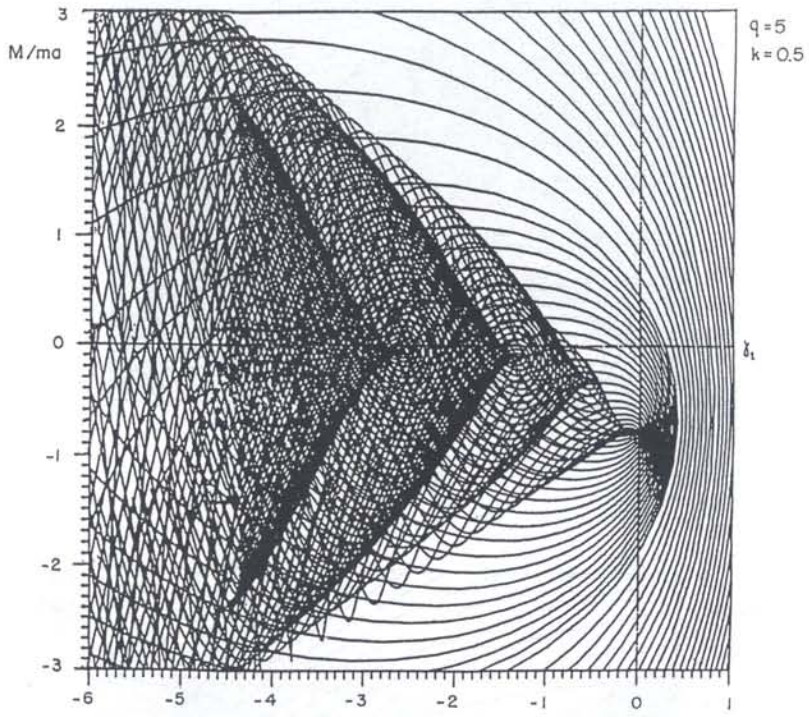

Fig. 22

Now in case of thermoelastic problems when temperature field T is isotropic, being an even function of ζ (along the plate thickness) and does not depend on ρ, then condition (23) describes the immovable hinge support where $\gamma_1 = \alpha^2 \kappa^2 \lambda^2 N_T / h^2$ (cf. Table 1). Then the basic equations (5), (6) do not contain terms explicitly depending on T, because $N_T = \text{const}$; $M_T \equiv 0$; $\lambda = 1$. The effect of temperature is transmitted only through boundary condition (23) ($\gamma_1 > 0$ means cooling and $\gamma_1 < 0$ heating). Thus both problems mentioned above are solved simultaneously by the same maps. Of course, there are no difficulties in considering a general thermoelastic problem for any function $T(\rho, \zeta)$. This will introduce linearly some additional terms in the basic equations and boundary conditions.

Now we can pass on the analysis of the above-given series of maps. This analysis means investigations of the topological structure of the maps in order to find relations between topology and physical behavior of the system considered. In brief, we must learn to read the map as, for example, a physician reads an X-ray photograph.

We shall begin comparing the maps in Figs. 21 ($q = 0$) and 18 ($q = 30$). First of all, the distribution of the series of cusp point A, B, C, ... (see Fig. 21), ordered for $q = 0$ on a straight line (horizontal axis $M = 0$), gets a new, very complicated, knotty character (Fig. 18). The first cusp (point A in Fig. 21) and its neighborhood move down when q increases (compare Fig. 21 and 18) but they remain topologically invariant (see region A in Fig. 18).

A different behavior is associated with "higher" cusps (B, C, ..., Fig. 21) and their neighborhoods. Fig. 18 shows the effect of accumulation of former higher cusps, and geometrical distortion and superimposition of their neighborhoods in a bounded region P of the map above point A (see Fig. 18).

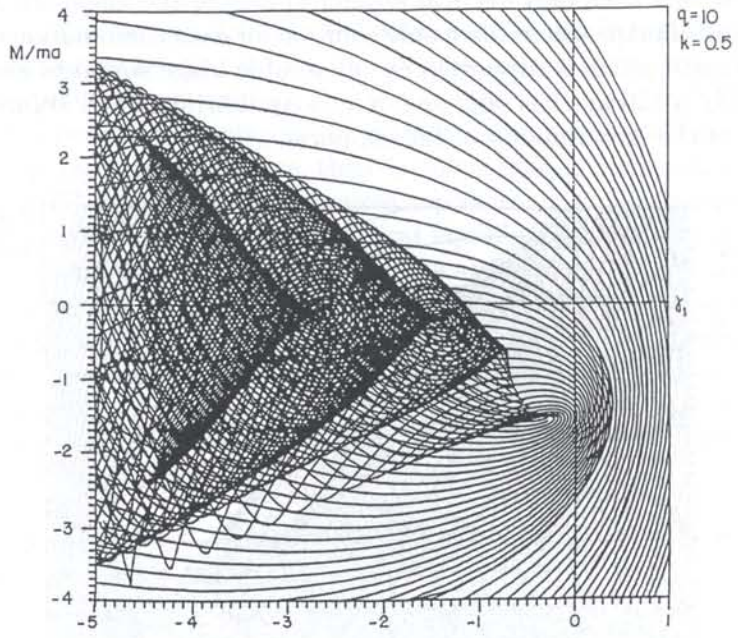

Fig. 23

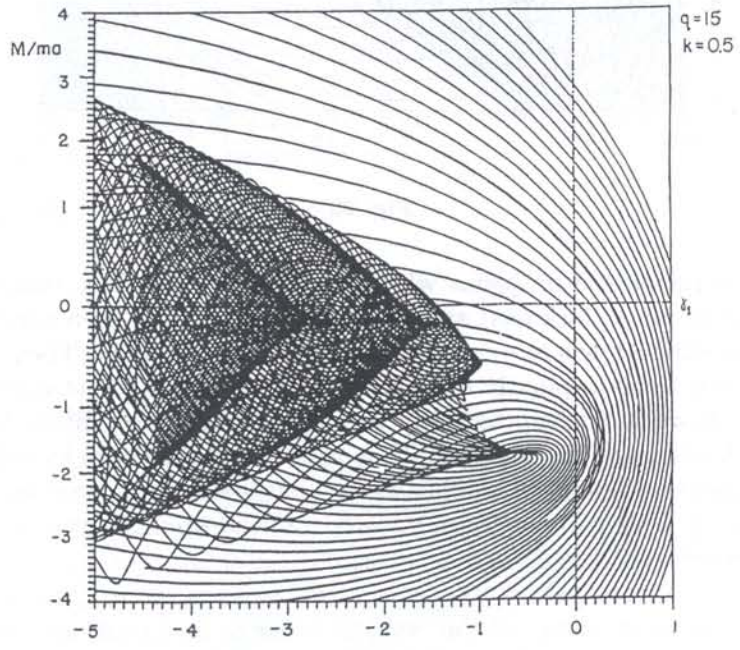

Fig. 24

Due to this accumulation phenomenon new singular points appear (e.g. labelled in Fig. 18 by S). The latter seems to correspond to the hyperbolic umbilic type of catastrophes [48]. Region P is not reflected fully in Fig. 18 because of its complexity. Even in a simplified form, this region has a very complex structure because the accumulated cusps change their character due to their nonlinear interaction during the accumulation process. It is clear that the former infinite spectrum of cusps A, B, C, ..., will not completely accumulate in region P above-described. That is way it is worthwhile to consider some section of the last map. Firstly, we note that the boundaries of cusp A region and area P (Fig. 18) determine the stability boundaries of the plate. Outside these

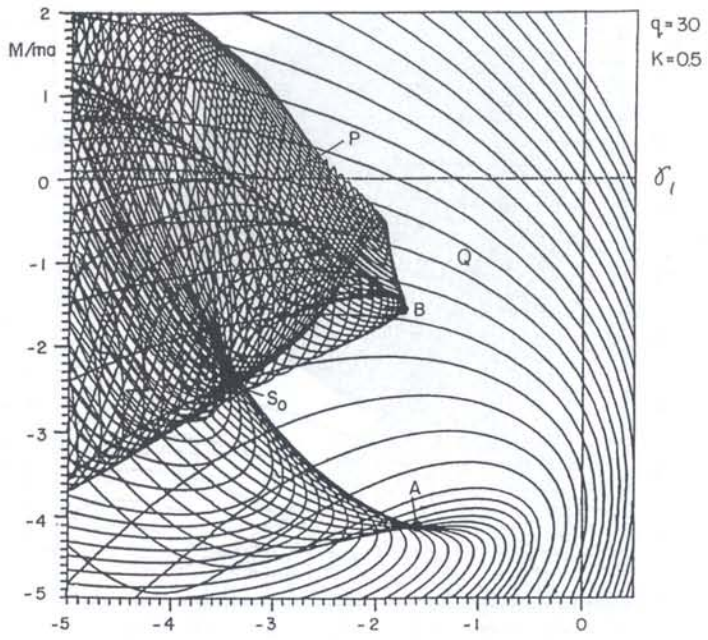

Fig. 25

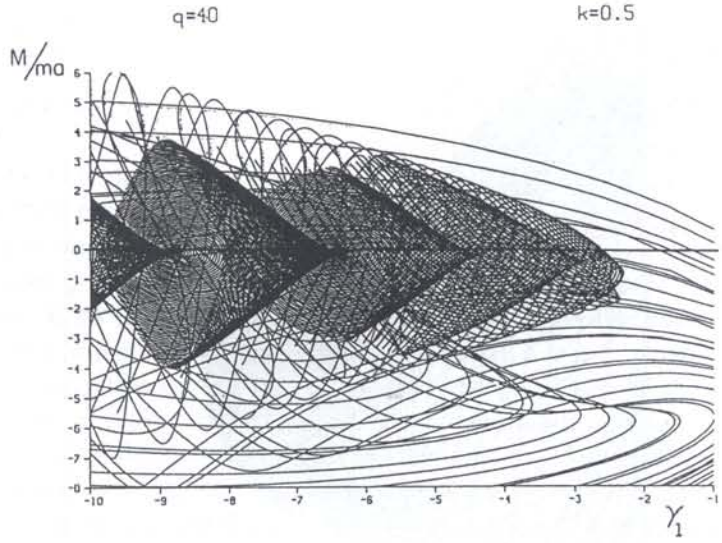

Fig. 26

regions (see area R in Fig. 18), there is only a single possible equilibrium state of the plate for each pair of M and N values. The map topography shows that each section obtained by a vertical line ($\gamma_1 = \text{const.}$) completely located in R will give a monotonic deformation curve (load-displacement curve) in plane ξ,M, where $\xi = \xi(0)/h$ — dimensioneless displacement of the plate center. If line $\gamma_1 = \text{const.}$ crosses the boundaries of region of cusp A and P, (that is, when the value of γ_1 lies approximately in the interval — $3.4 < \gamma_1 < -1.6$) there is, as expected, and additional separate closed loop of the deformation curve, because of the A and P regions structures. If $\gamma_1 < -3.4$, then the corresponding deformation curves (map section $\gamma_1 = \text{const.}$) have a complicated continuous character.

In Fig. 19 examples of deformation curves for different γ_1 are given ($\gamma_1 = -1, -1.5, -3$). Two other cases ($\gamma_1 = -2; -3.5$) are presented in Figs. 29 and 30. It can be seen that for $\gamma_1 = -3.5$

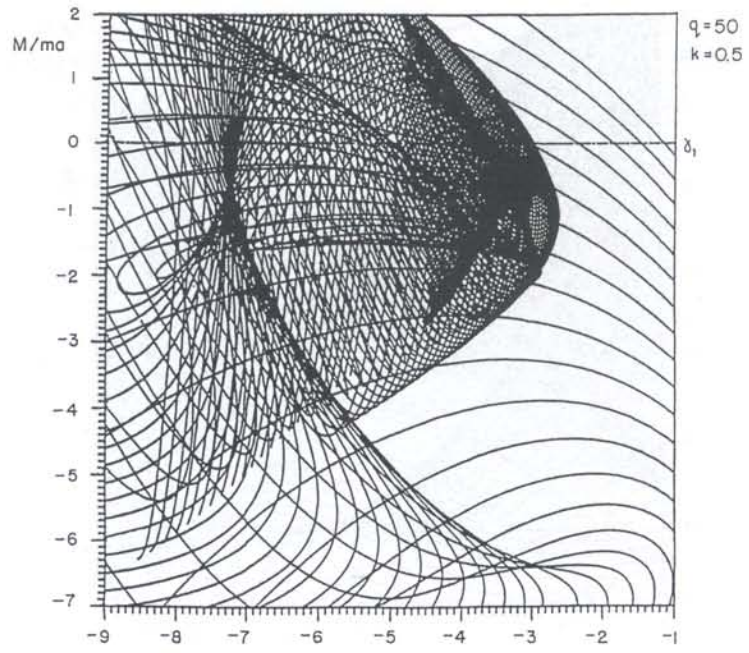

Fig. 27

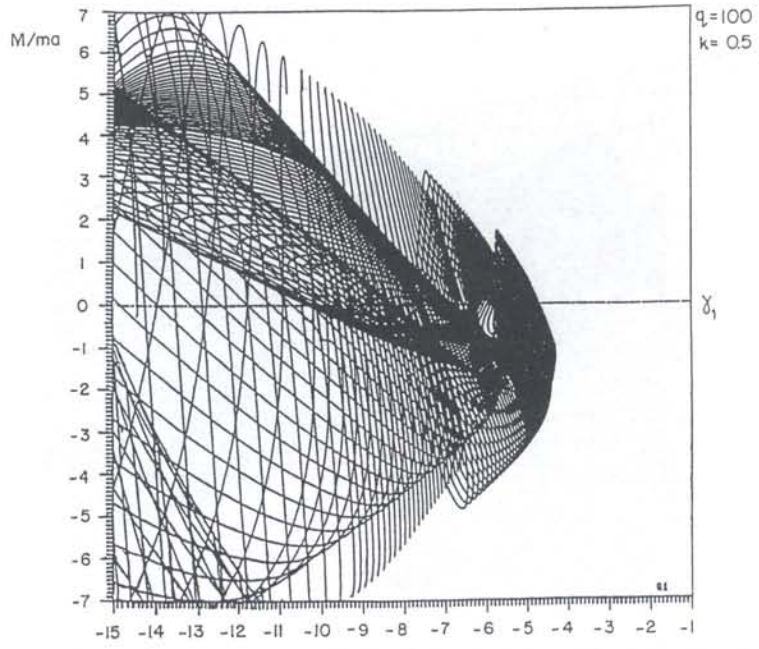

Fig. 28

the former separate loop is again coupled with the "classical three-valued" curve forming a new very complicated deformation curve. All states corresponding to points on solid lines shown in the last three figures are stable, and those on the crossed out lines are unstable. The method and appropriate algorithm for testing the stability of equilibrium states are described in [44]. Thus there are two bifurcation values of γ_1 (about $\gamma_1 = -1.6$ and -3.4) when a separate loop appears and disappears, respectively.

The existence of loop L means, as mentioned above, that there is no continuos transition from states corresponding to the points on the 'open' curve 0 (see Fig. 19). From Fig. 18, it can be

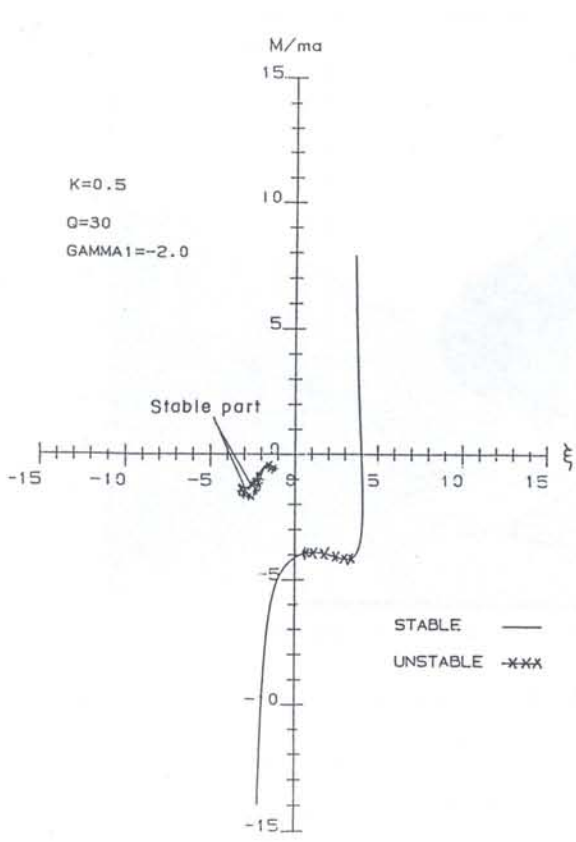

Fig. 29

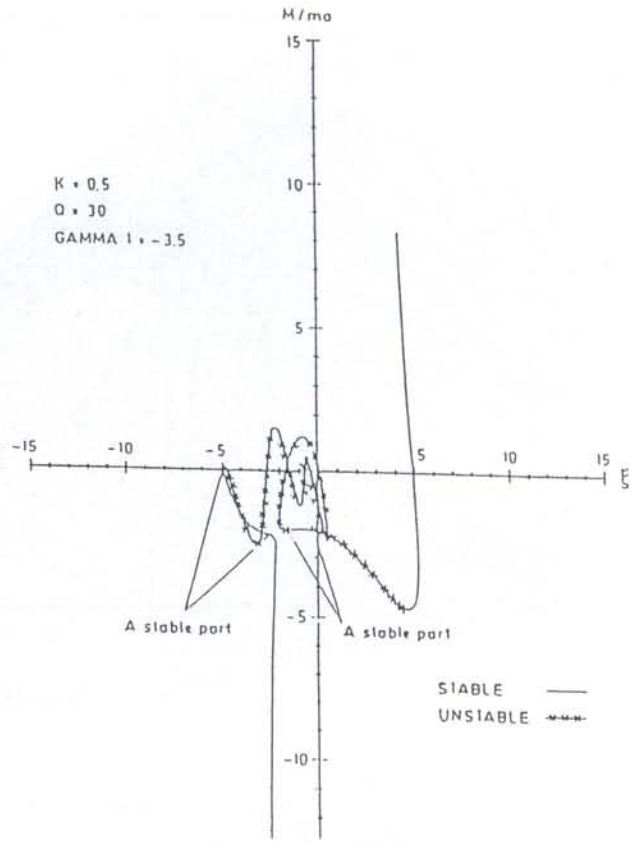

Fig. 30

concluded that, in the P region of the map, at least four cusps are accumulated. (The number of equilibrium states which correspond to a fixed value M can be equal to nine - eight marked by points on the loop, and one on curve 0).

Comparison of cases $q = 0$ and 30 shows that q is the main control parameter determining the stability behavior. This is why it is very important to trace the dynamics of change of the deformation map as the value of q increases. It is clear that when q increases, the first cusp goes down, while the third and subsequent cusps approach the boundary of the second one where the process of accumulation of higher cusps begins. This accumulation effect can be clearly seen in Fig. 25 for $q = 30$ (this figure differs Fig. 18 by the scale, and enables clarification of some important details of the map connected with the cusps' accumulation).

Figures 28 and 31 represent maps for $q = 100$ on two different scales. (due to their complexity, these presentation are incomplete. For example, the series of parabola-like curves of the type labeled by letter Q in Fig. 25 are not shown in the zone of cusps' accumulation presented in Figs. 28,31). Comparing maps for different values of q, one can notice that the increase of q results in significant intensification of the process of accumulation and nonlinear interaction of the higher cusps. These maps are of more complex structures. For $q = 100$ it seams that the corresponding map already gains an unpredictable, chaotic character. In order to confirm this conjecture, Figs. 32 and 33 are presented. They give different details of the region of accumulation for $q = 100$. The unpredictable chaotic character of plate's static behavior is very clearly demonstrated by different parts (also incomplete) of the deformation map for $q = 100$ presented in Figs. 34, 35 and 36.

Figure 34 is associated with interval $(-12 < \gamma_1 < -8)$. The part of the map for $(16 < \gamma_1 < -12)$ is shown in Fig. 35 and Fig. 36 represents the behavior of the system when $(-20 < \gamma_1 < -16)$. The discussion about chaotic behavior in statics, which is still to be clarified, is provided in [38].

Thus the use of the global tool (map) is serves to explain the physical meaning of the topological structure of the map. Or, in order words, to establish the connection with the topology of different

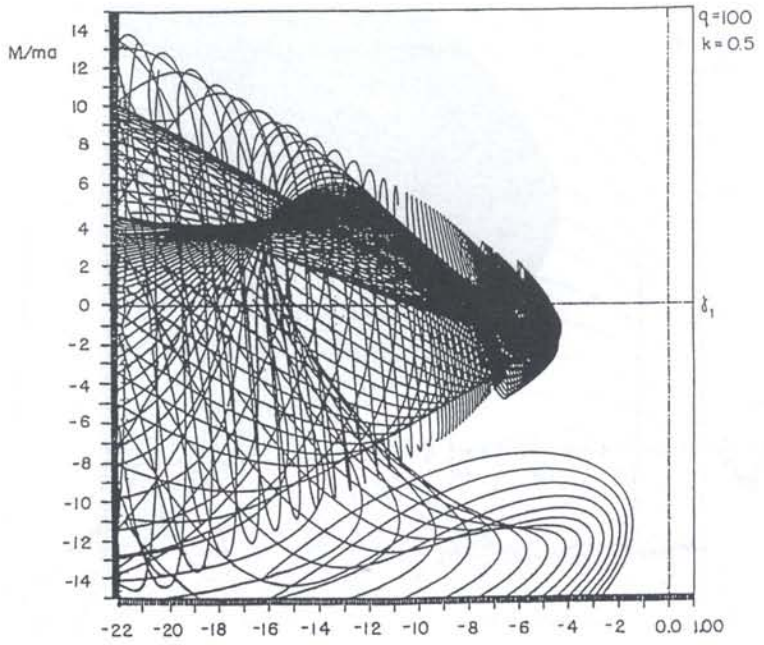

Fig. 31

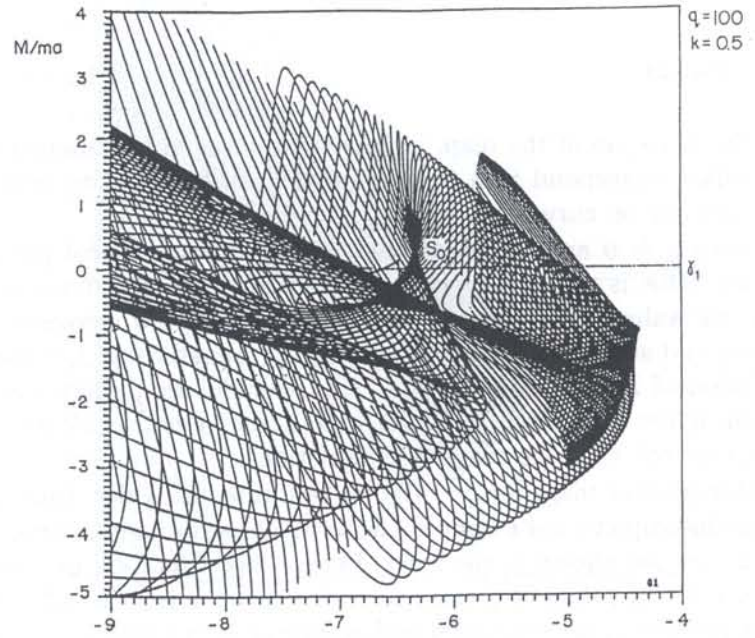

Fig. 32

areas of the map and the response of the plane to different values of the considered three parametric loadings. The most important elements of this topology are the boundaries (envelopes) of regions with of different degrees of nonuniqueness of solutions and the isolated singular points. The latter are cusp points and singular points which are knots of many lines. Such singular points are labeled in the maps by S_0. Thus the above-mentioned basic elements of topology are indicators of change of the map's structure and in consequence the behavior of the plate. We shall try now to see what we know about the physical role (interpretation) of these basic elements.

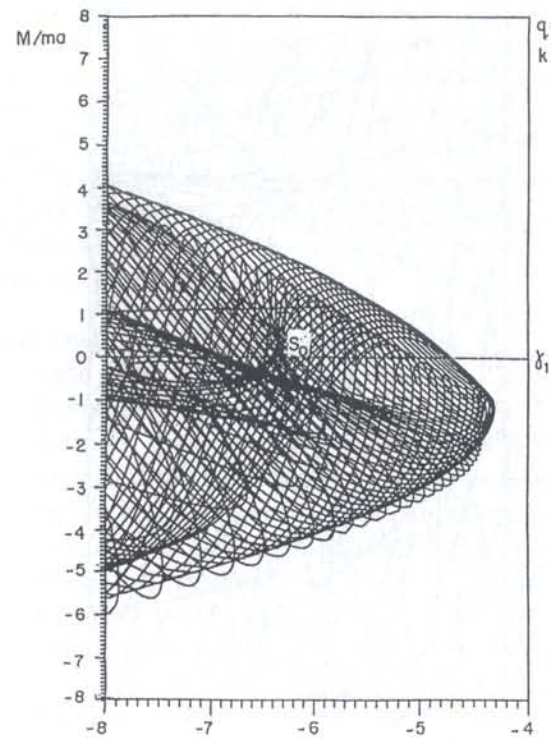

Fig. 33

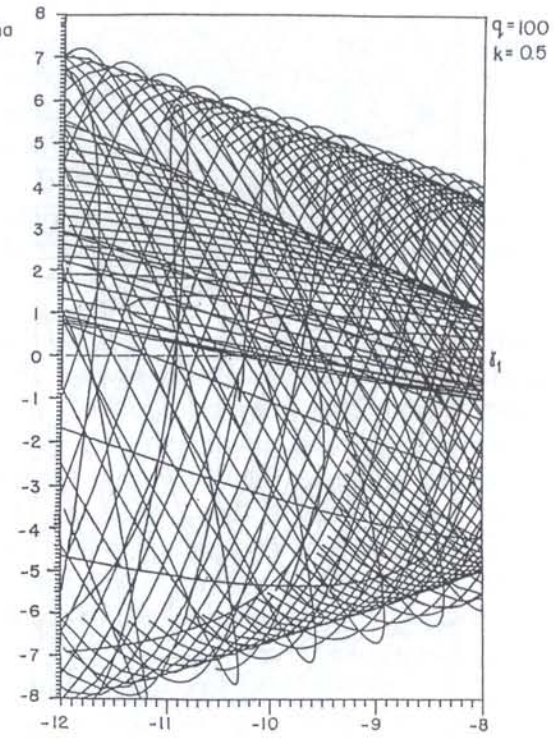

Fig. 34

First of all we can see that all the envelopes (which are boundaries crossing of which changes the degree of multitude (nonuniqueness) of the solutions) are finished by a cusp corner. An exception here is the "front" boundary of the zone of accumulations of the higher cusps for some q, which is rounded and curves without any "cogs". Such a front is available in the map in Fig. 27 for $q = 50$ where the corresponding area is above the lowered first cusp. On the other hand, the upper part of the front of the map for $q = 30$ (Fig. 25) does not contain "teeth", but is not rounded. The front of the map for $q = 40$ has "teeth" (Fig. 26). Formation of an unrounded front or with teeth is understable because this front is a result of accumulations of different cusp areas, where each of them has a triangular form with a sharp corner (cusp). The existence of a rounded boundary of the front is not clearly understood and from the available data it seems to be an exception.

In order to analyze the physical meaning of different values of γ_1. We shall begin, for example with case $q = 30$ (Fig. 25). Let $\gamma_1 > \gamma_A$ (where γ_A corresponds to the first cusp — see point A in Fig. 25). In this case section $\gamma_1 = \text{const.}$ lies in the area where only a unique solution exists (see the monotonical curve for $\gamma_1 = -1$ in Fig. 19). At $\gamma_1 = \gamma_A \approx -1.5$ (Fig. 19) the deformation curve has a point of inflexion in the middle and for $|\gamma_1| > 1.5$ the solutions cease to be unique, and their number depends on which areas specific line $\gamma_1 = \text{const.}$ pass through. When $\gamma_B < \gamma_1 < \gamma_A$ (B is the most advanced point of the upper front — see Fig. 18) there are three solutions and a typical (classical) deformation curve with one maximum and one minimum (snap-through loss of stability). The upper (lower) critical value of the moment in the ordinate of the upper (lower) point of intersection of line $\gamma_1 = \text{const.}$ with the boundaries of "triangular" area with A vertex (see Fig. 25). Now if line $\gamma_1 = \text{const.}$ lies in the range $|\gamma_1| < \gamma_1 < |\gamma_{S0}|$ (where γ_{S0} is the abscissa of singular point S_0), then it will intersect two areas of the map with nonunique solutions — the above-mentioned "triangular" area with peak A and area labelled in Fig. 25 by P where accumulation of the higher cusps takes place. As a results, deformation curve which corresponds to such a section of the map will have a complex character, being composed of a "classical" curve with three solutions (one maximum and one minimum) and, in addition, a separate closed loop. (See Fig. 19 — curve labelled by 0 and loop L for $\gamma_1 = -3$, and a similarly composed deformation curve for $\gamma_1 = -2$ presented in Fig. 29).

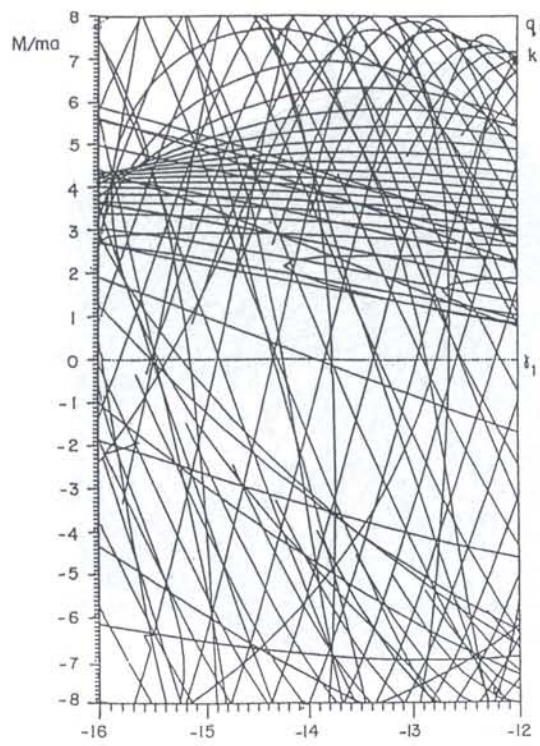

Fig. 35

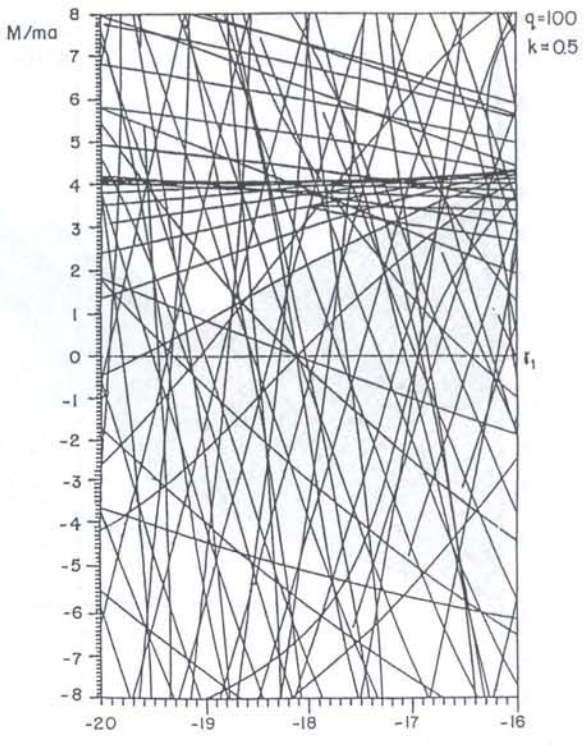

Fig. 36

In both Figs. 19 and 29 the point denoted by x represents unstable states. Then a part of these loops is stable. This means that beside the usual snap-through loss of stability process at limit points another jump type process of stability loss with transition from one stable state on the curve 0 to another state on the stable branch of the loop L and vice versa can happen. The latter case can take place if an additional external energy is introduced. For example a heating blow, that is an increase in $|\gamma_1|$, will transfer by jumping from a stable state on curve 0 (in a range of M where the loop exists) to the corresponding stable state on the loop and vice versa in the case cooling. But if the equilibrium state on the loop corresponds to one of its limit points (the end points of the loop stable branch are limit points), then the loss of stability by jumping will take place in a normal way without any additional energy. Moreover, during this process a portion of deformation energy will be lost as in a usual snap-through process because transition from a prebuckling state (which has a high energy) to postbuckling state which is stable (and which possesses less energy than prebuckling) will take place.

It is necessary to emphasize that these phenomena cannot be overestimated. By any incremental approach which is an integral part of finite elements and finite difference methods or of other methods of this type, separate loops or branches cannot be found if they are not known a priori. But the sections of our deformation maps can show these loops or separate branches automatically without any special approaches or means. The dynamics of the change of complex (with loops) deformation curves when $|\gamma_1|$ increases (in the considered interval $(|\gamma_1|, |\gamma_{S0}|)$) and then it can be seen that the sizes and complexity of loop shapes grow. The "distance" between the loops and the classical parts of deformation curves also diminishes. The difference between the upper and lower critical values of M on parts 0 also increases together with the increase in $|\gamma_1|$.

All these phenomena can be readily seen by comparing Figs. 19 and 29. They show that joining of the two distinct parts (0 and L) of deformation curve can be expected when $|\gamma_1|$ increases. Indeed, this event takes place when $|\gamma_1| = |\gamma_{S0}|$ and after this ($|\gamma_1| > |\gamma_{S0}|$) the loops disappear forming together with line 0 a new complicated continuous curve. See Fig. 30 for $\gamma_1 = -3.5$, which is very close to value γ_{S0}.

Here the following phenomenon takes place. In all the previous cases there were not more than two stable states for each value of M and γ_1 . This very important fact was established after a wide series of solutions in case of a single parameter loading (see [18, 20, 21, 32]) and also for some cases of two parameter loading (see Fig. 12, for example). But in case $\gamma_1 \approx -3.5$ (Fig. 30) there are for $M/m_\alpha \approx 3$ three stable states. Here this phenomenon is demonstrated very weakly since it is "on the boundary", but for greater values of q ($q = 50$ and more) it was confirmed very clearly in [49–51] when $|\gamma_1|$ increases, and after passing over the value of $|\gamma_{S0}|$ there will again be only two stable states [49–51]. Summarizing, we can see that the following basic features were established in the considered case.

(a) The cusps (singular points A, B, C, ...) are very neat regular and symmetrically ordered in case of plate when $q = 0$ (see Figs. 21, 14); when q is increased the map loses its symmetry and becomes more and more complicated reaching the following topological structure (in general terms). The first "triangle" area with vertex A, goes down remaining topologically invariant (which is the same feature of three solutions for each γ_1) and with a bent boundary but forming, as previously, ($q = 0$), an "angle" with vertex A. The other (higher) cusps' areas begin to accumulate in the front, forming a new area with a new boundary where nonuniqeuness of solution is reached (see the region with the advanced point B in Fig. 25). This new boundary together (with the boundary of the first "angle" A of the firs (invariant) cusp area defines the boundaries of stability, where outside (right side) is the area of unique (stable) solutions. The compound boundary is complicated, being partly convex (relative to the stable area) and partly concave. Thus the known theorem about convexity of the boundary of stability in case of linear stability (the prebuckling mode is a solution of a linear problem) is not valid in general for nonlinear systems.

(b) Between the two areas described above of the map these is a part of the stable area labeled T in Fig. 25 which is a convex (relative to the stable area) boundary the shape of which is similar to sign $<$ (the same can be seen in maps Figs. 26–28). Such a type of area forecasts the existence of separate loops in the deformation curve $M(\xi)$ which are obtained by section $\gamma_1 = \text{const.}$ of the map, which intersect the zone with the $<$ boundary described above. In general it was observed [49] that when there exists a boundary which joins two cusp regions by a curve of shape similar to $<$ or C there will appear separate loops in the sections where $\gamma_1 = \text{const}$. This can be found even inside the zone of higher cusps accumulation.

In maps for interval $0 < q \leq\approx 40$ inequality $\gamma_A > \gamma_B$ is valid (see for example Fig. 25). When $q \approx 40$, we have $\gamma_A \approx \gamma_B$ and after this ($q > 40$) the value of γ_A is less than γ_B. In consequence vertical line $\gamma_1 = \text{const}$, which moves from right to left, beginning from the stable area, will meet, first of all, point B and will enter the zone of cusps accumulation not intersecting the cusp area with vertex A. As can be shown [49, 51], in this case the corresponding deformation curve $M(\xi)$ consists of a classical whole stable monotonic curve (without extremal — limit points) and separate loops which are the classical line reaches extremal (limit) points and part of a separate loop becomes instable. When $\gamma_1 = \gamma_A$, the classical curve has a point of inflexion with a horizontal tangent. Thus we have clarified the role of each area in the frontal part of the map and its boundary in the process of describing the global behavior of plate.

(c) At the first (moving along axis γ_1 from right to the left) singular point of types S_0 where a separate loop will join the classical curve forming a very knotty deformation curve $M(\xi)$. In the neighborhood of γ_{S0} there exist three stable states. This is the role of singular point S_0. For relatively small q, e.g., when $q < 15$, neither such singular points nor separate loops were observed. For $|\gamma_A| \gg |\gamma_{S0}|$, i.e., very far left from $|\gamma_{S0}|$, the corresponding part of the map remains almost ordered, being similar to type S_0 or of other types which have not yet been investigated. As, for example, when $q = 100$, we can see the singular point of type S_0 when $\gamma_1 \cong -6.4$ in Fig. 32 and 33, and another singular point in the region of point $\gamma_1 = -15.8$, $M/m_\alpha \approx 4.3$ (see Fig. 31 and 35).

(d) All the above shows that pressure q is the main control parameter and that it is the basic parameter which controls the behavior of plate.

(e) It is worth noting that line $\gamma_1 = 0$ lies completely in the area of stability where a unique solution exists, independent of the magnitude of q. This is an interesting and important fact, the meaning of which is not trivial, as it might seem at first glance. Suppose, for example that only M is acting, then the deformed plate reaches the shape of a cap of revolution (shown qualitatively in Fig. 37a). Now if pressure q is added (as shown in Fig. 37b), we can suppose the existence of jumping, that is, transfer to a new state, and in consequence the solution for given magnitudes of

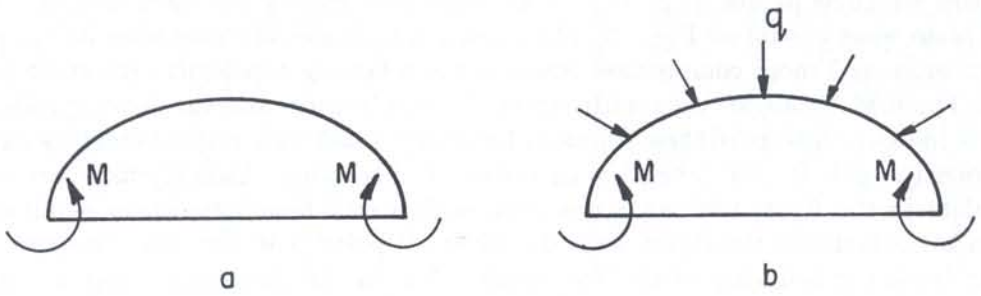

Fig. 37

M and q is not unique. But this can never happen because when q increases, the nonstable area of the map goes away from line $\gamma_1 = 0$. Closest to this line is the area of instability when $q = 0$, but this area has no common points with line $\gamma_1 = 0$. This fact was well proved mathematically in [36] for isotropic case. It is a consequence of the positiveness of membrane function $\omega(\rho)$ on $(0 \leq \rho \leq 1)$, and this circumstance insures the uniqueness of the solution. The map confirms this important feature in the orthotropic case also. Of course the considered feature is related to axisymmetrical deformation under M, when $q = 0$ and this does not exclude loss of stability by bifurcation in tension with a transition into an asymmetrical form.

4. Conclusions

In conclusion it is worth to paying attention to the following aspects:

i) The deformation map is not only a tool global investigation of the behavior of a considered system but it is a very valuable concentration of information necessary for optimal design and other diverse applications.

ii) We did not consider the problem of the influence of loading paths on nonlinear systems behavior. This problem was investigated theoretically in [52].

iii) Further topics for investigation are bifurcation phenomena which lead to asymmetrical deformations and dynamic problems.

References

[1] L. Euler. *Methodus inveniendi lineas curvas maximi minimive proprietate gaudentes.* Appendix 1. De curvis elastice (in Latin). Lausanne and Geneva, 1744.

[2] L. Euler. Sur la force de colonnes (in French). *Mem. Acad. Roy. Sci. et Belles Lettres*, Berlin, 13: 251–282, 1757.

[3] S. Timoshenko. *History of Strength of Materials.* McGraw-Hill Co., N.Y., 1953.

[4] L. Cesari. *Asymptotic behavior and stability problems in ordinary differential equations.* Springer Verlag, Berlin–Göttingen–Heidelberg, 1959.

[5] H. Ziegler. *Principles of Structural Stability.* Blaisdell Publ. Co., Toronto, London, 1968.
[6] A.A. Andronov, L.Pontryagin. Large Systems (in Russian). *Dokl. AN SSSR*, **14**: 247–251, 1937.
[7] V.I. Arnold. *Mathematical Methods of Classical Mechanics.* Springer-Verlag, N.Y., 1978.
[8] R. Thom. *Structural Stability and Morphogenesis.* W.A. Benjamin Inc., Massachusetts, 1974.
[9] J. Argyris, G. Faust, M. Haase. *An Exploration of Chaos.* North Holland, Amsterdam, 1994.
[10] H. Poincaré. Sur l'équilibre d'une masse fluide animé d'un mouvement de rotation (in French). *Acta Mathematica*, **7**: 259–290, 1885.
[11] H. Poncaré. *Figure d'equilibre d'une masse fluide* (in French). Ed. C.Naud, Paris, 1902.
[12] V.I. Arnold. Lectures on bifurcation in versal families. *Russian Math. Survey*, **27**: 54–123, 1972.
[13] G. Ioss, D.D. Joseph. *Elementary Stability and Bifurcation Theory.* Springer Verlag, 1980.
[14] M. Golubitsky, D.G. Schaeffer. *Singularities and Groups in Bifurcation Theory.* Vol.1, Springer-Verlag, 1985.
[15] W.T. Koiter. *Over de stabiliteit ran het elastisch evenwicht* (in Dutch). Thesis Doc.Delft, 1945. English transl. NASATT F-10, 833, 1967; AFFDL-TR-70-25, 1975.
[16] W.T. Koiter. Elastic Stability and Post-Buckling Behaviour. In: R.E. Langer, ed. *Nonlinear Problems*, 257–275. Symp. Univ. of Wisconsin, Univ. of Wisconsin Press, Madison, 1963.
[17] K. Husein. *Vibration and Stbility of Multiple Parameter Systems.* Noordhoff Int. Publ., Alphen aan den Rijn, 1978.
[18] D. Shilkrut. Solution of some stability problems in the theory of geometrically non-linear shells. *Isr. J. of Techn.*, **18**: 76–83, 1980.
[19] E. Ramm. Strategies for tracing the nonlinear response near limit points. *Nonlinear FEM analysis in structural mechanics.* Proc. of the Europe-USA workshop, Ruhr-Univ. Bochum. Springer Verlag, 1981.
[20] D.I. Shilkrut, P.M.Vyrlan. Stability of Nonlinear Shells (in Russian). *Polytech. Inst. Kishinev*, 1977. Transl. into English by US Air Force FID-ID (RS) T-02046079, 1979.
[21] D.I. Shilkrut, P.M. Vyrlan. Stability and geometrically nonlinear shells (in Russian). *Dokl. Acad. Nauk SSSR*, **225**, 1975. Engl. transl. *Soviet Phys. Dokl.*, **20**: 865–867, 1976.
[22] S.P. Timoshenko, J.M. Gere. *Theory of elastic stability.* McGraw-Hill, 1963.
[23] N.-C. Huang. Unsymmetrical buckling of thin shallow spherical shells. *J.Appl.Mech.* **31**: 447–457, 1964.
[24] J.R. Fotch, B. Budiansky. Buckling and postbuckling behavior of spherical caps under axisymmetrical load. *AIAAJ.*, **8**: 686–693, 1970.
[25] J.R. Fitch. The buckling and postbuckling behavior of spherical caps under concentrated load. *Int. J. Solids and Structures*, **4**: 421–426, 1970.
[26] L. Bauer, E.L. Reiss, H.B. Keller. Axisymmetric buckling of hollow spheres and hemispheres. *Comm. Pure Appl. Math.*, **23**: 529, 1970.
[27] J.C. Wohlever. *A group theoretic approach to the nonlinear bifurcation analysis of shells of revolution.* PhD Dissertation, Cornell Univ., August, 1993.
[28] K. Huseyin. *Nonlinear theory of elastic stability.* Noordhoff, The Netherlands, 1975.
[29] K. Huseyin. *Multiple-parameter stability theory and its applications.* Oxford Univ. Press, 1986.
[30] L.S. Cheo, E.L. Reiss. Unsymmetric wrinkling of circular plates. *Quart. Appl. Math.*, **31**: 75–91, Apr. 1973.
[31] D. Shilkrut, E. Kochavi. Asymmetrical bifurcation phenomena in geometrically nonlinear spherical caps subjected to multiparametric loading. *Thin Walled Str.*, **4**: 83–99, 1986.
[32] D.I. Shilkrut, P.M. Vyrlan. On the stability of symmetric forms of equilibrium of geometrically nonlinear shells of revolution (in Russian). *Sci. Annual Issledowanya po teorii soorujeniy*, **22**: 104–113, 1976.
[33] Ta-Cheng Loo, R.M. Evan-Iwanowski. Interaction of critical pressure and critical concentrated loads acting on shallow spherical shells. *J. Appl. Mech.*, Sept.: 612–616, 1966.
[34] A.S. Volmir. *Stability of Elastic Systems* (in Russian). Fizmatgiz, Moscow, 1963.
[35] N. Yamaki. *Elastic Stability of Cylindrical Schells.* North-Holland, 1984.
[36] D. Shilkrut. *Problems of the quantitaive theory of nonlinear shells* (in Russian). Shtiyntza, Kishinev, 1974.
[37] D. Shilkrut. The deformation map as a means for investigating the behavior of deformable nonlinear bodies. *Mech. Res. Com.*, **9**: 77–84, 1982.
[38] D.I. Shilkrut. Stability of equilibrium states of nonlinear structures and chaos phenomena. Chaos in statics? *Int. J. of Bifurcation and Chaos*, **2**: 271–283, 1992.
[39] Y. Stavsky. Nonlinear theory of axisymmetric deformations of heterogeneous shells of revolution. In: D.Abir, ed., *Contribution to Mechanics*, p. 18. Perrgamon Press, Oxford, 1970.
[40] S.A. Ambartsumyan. *The general theory of anisotropic shells* (in Russian). Nauka, Moscow, 1974.
[41] S.G. Lekhnitskiy. *Theory of anisotropic elastic body.* Holden-Day, San Francisco, 1963.
[42] D. Shilkrut. Investigations of axisymmetrical deformation of geometrically nonlinear, rotationally orthotropic, circular plates. *Int. J. Nonlinear Mechanics*, **18**: 95–118, 1983.
[43] K.O. Friedrichs, J.J. Stoker. Buckling of the circular plate beyond the critical thrust. *J. Appl. Mech.*, **9**: 7–14, 1942.
[44] D. Shilkrut. Stability and vibrations of geometrically nonlinear cylindrically orthotropic circular plates. *J. Appl. Mech.*, **51**: 354–360, 1994.

[45] H.B. Keller, A.W. Wolfe. On the nonunique equilibrium states and buckling mechanism of spherical shells. *J. Society Ind. Appl. Math.*, **13**: 674–705, 1967.

[46] D.I. Shilkrut, N.V. Shevandronov, V.P. Morar, Yu.A. Maksimov. Analog computer solution of problems in nonlinear shell theory by direct simulation and digital computation of these problems by direct reduction to a Cauchy problem (in Russian). *Publ. of AN Mold. SSR*, Kishinev, 1969.

[47] P.F. Papkovitch. *Works on navy structural mechanics* (selected works), Vol.4 (in Russian). Sudpromgiz., Leningrad 1963.

[48] A.E.R. Woodcock, T. Poston. *A geometrical study of the elementary catastrophes.* Springer Verlag, 1974.

[49] R. Eshkenazi. *Stability of nonlinear deformed system.* MS degree thesis (advisor Prof. D. Shilkrut). Ben-Gurion University of the Negev, 1995.

[50] D. Shilkrut, R. Eshkenazi. Some aspects of buckling by snap-through phenomena of geometrically nonlinear structures. (In press).

[51] D. Shilkrut. About the ways of stability loss by snap-through of geometrically non-linear shells (systems) and some related problems, *Int. J. Non-Linear Mech.*, **29**: 671–686, 1994.

[52] D. Shilkrut. On the influence of the paths of conservative multiparametric loading on equilibrium states of geometrically nonlinear structures. *Computers and Structures*, **44**: 137–146, 1992.